Anisotropic a posteriori error estimate for the virtual element method

IMA Journal of Numerical Analysis (2021) Page 1 of 32
doi:10.1093/imanum/drnxxx

Anisotropic a posteriori error estimate for the Virtual Element Method

P. F. ANTONIETTI†
MOX, Dipartimento di Matematica, Politecnico di Milano, Italy

AND

S. BERRONE‡, A. BORIO§, A D'AURIA¶
Dipartimento di Scienze Matematiche, Politecnico di Torino, Italy

AND

M. VERANI‖
MOX, Dipartimento di Matematica, Politecnico di Milano, Italy

AND

S. WEISSER∗∗
Universität des Saarlandes, Germany

[Received on 7 January 2021]

We derive an anisotropic a posteriori error estimate for the adaptive conforming Virtual Element approximation of a paradigmatic two-dimensional elliptic problem. In particular, we introduce a quasi-interpolant operator and exploit its approximation results to prove the reliability of the error indicator. We design and implement the corresponding adaptive polygonal anisotropic algorithm. Several numerical tests assess the superiority of the proposed algorithm in comparison with standard polygonal isotropic mesh refinement schemes.

Keywords: Virtual Element Method; anisotropy; a posteriori error analysis.

1. Introduction and Notation

In recent years, the numerical approximation of partial differential equations on computational meshes composed by arbitrarily-shaped polygonal/polyhedral (polytopal, for short) elements has been the subject of an intense research activity. Examples of polytopal element methods (POEMs) include the Mimetic Finite Difference method, the Polygonal Finite Element Method, the Polygonal Discontinuous Galerkin Finite Element Method, the Hybridizable Discontinuous Galerkin and Hybrid High-Order Methods, the Gradient Discretization method, the Finite Volume Method, the BEM-based FEM, the Weak Galerkin method and the Virtual Element method (VEM). For more details see the special issue Beirão da Veiga & Ern (2016) and the references therein.

The novelty and recent surge of interest in POEMs stems from their ability to describe a physical domain using not only standard shapes (triangles, tetrahedra, square, hexahedra,...) but also highly irregular and arbitrary geometries. This flexibility of essentially arbitrary polytopal meshes is naturally very attractive for designing adaptive algorithms based on mesh refinement (and derefinement/agglomeration) driven by suitable a posteriori error estimates. However, while (isotropic and anisotropic) error estimates and a posteriori error estimates and adaptive finite element methods (AFEMs) have been intensively investigated during the last decades (see, e.g., for the isotropic case the monographs Verfürth (2013); Nochetto & Veeser (2012) and the references therein and for the anisotropic case Apel (1999); Formaggia & Perotto (2001, 2003); Georgoulis (2003, 2006); Georgoulis *et al.* (2007a,b) and the references therein), the corresponding

†Email: paola.antonietti@polimi.it
‡Email: stefano.berrone@polito.it
§Corresponding author. Email: andrea.borio@polito.it
¶Email: alessandro.dauria@polito.it
‖Email: marco.verani@polimi.it
∗∗Email: weisser@num.uni-sb.de

study of a posteriori error estimates and adaptivity for polytopal methods is still in its infancy. See, for example, Beirão da Veiga (2008); Beirão da Veiga & Manzini (2008); Antonietti *et al.* (2013) for the study of a posteriori error estimates in the context of Mimetic Finite Differences, Beirão da Veiga & Manzini (2015a); Berrone & Borio (2017); Cangiani *et al.* (2017b); Mora *et al.* (2017); Beirão da Veiga *et al.* (2019); Chi *et al.* (2019); Cangiani & Munar (2019) for the Virtual Element Method, Weisser (2011); Weisser (2017); Weisser & Wick (2018); Weisser (2019) for polygonal BEM-based FEM, Zenoni *et al.* (2017) for the polygonal Discontinuous Galerkin method, Di Pietro & Specogna (2016) for the Mixed High Order method, Mu (2019) for the Weak Galerkin method and Vohralík & Yousef (2018) for lowest-order locally conservative methods on polytopal meshes. Moreover, despite the great flexibility provided by polytopal meshes, the above works focused on the isotropic case, only. The anisotropic adaptive polytopal mesh refinement, to our knowledge, has been addressed only in Antonietti *et al.* (2019) for the Virtual Element Method in two dimensions. For completeness, see also the recent work Cao & Chen (2019) for nonconforming VEM *a priori* anisotropic error analysis. Aim of this paper is to push forward the research of Antonietti *et al.* (2019) providing a rigorous polygonal anisotropic *a posteriori* error estimate for conforming VEM and numerically assessing its efficacy in driving polygonal adaptive anisotropic mesh refinement strategies for the virtual element approximation of a paradigmatic two-dimensional elliptic problem.

The outline of the paper is as follows. In Section 2 we introduce the continuous elliptic problem together with its lowest order virtual element approximation. In Section 3 we first make precise the notion of *polygonal anisotropy*, then we state the anisotropic mesh regularity assumptions under which our theoretical results will be obtained. In the same section we also collect a series of instrumental results that will be employed in the subsequent analysis. In Section 4 we introduce a quasi-interpolant operator and prove approximation results that will be employed in Section 5 where a novel polygonal anisotropic a posteriori error estimate is obtained. Finally, in Section 6 we present a set of numerical results assessing the validity of our theoretical error estimates and the capability of our anisotropic error indicators to drive an adaptive polygonal anisotropic mesh refinement strategy for the solution of an elliptic problem.

1.1 *Notation of functional spaces and technical results*

We use the standard definition and notation of Sobolev spaces, norms and seminorms as given in Adams & Fournier (2003). Hence, the Sobolev space $H^s(\omega)$ consists of functions defined on the open bounded connected subset ω of $\mathbb{R}^2$ that are square integrable and whose weak derivatives up to order s are square integrable. As usual, if $s = 0$, we prefer the notation $L^2(\omega)$. Norm and seminorm in $H^s(\omega)$ are denoted by $\|\cdot\|_{s,\omega}$ and $|\cdot|_{s,\omega}$, respectively, and $(\cdot,\cdot)_\omega$ denote the L^2-inner product. The subscript ω may be omitted when ω is the whole computational domain Ω.

If $\ell \geqslant 0$ is an integer number, $\mathbb{P}_\ell(\omega)$ is the space of polynomials of degree up to ℓ defined on ω, with the convention that $\mathbb{P}_{-1}(\omega) = \{0\}$. The L^2-orthogonal projection onto the polynomial space $\mathbb{P}_\ell(\omega)$ is denoted by $\Pi_\ell^{0,\omega} : L^2(\omega) \to \mathbb{P}_\ell(\omega)$. The space $\mathbb{P}_\ell(\omega)$ is the span of the finite set of *scaled monomials of degree up to* ℓ, that are given by

$$\mathscr{M}_\ell(\omega) = \left\{ \left(\frac{\mathbf{x} - \bar{\mathbf{x}}_\omega}{h_\omega} \right)^\alpha \text{ with } |\alpha| \leqslant \ell \right\}, \tag{1.1}$$

where

- $\bar{\mathbf{x}}_\omega$ denotes the center of gravity of ω and h_ω its characteristic length, as, for instance, the edge length or the cell diameter for $d = 1, 2$;
- $\alpha = (\alpha_1, \alpha_2)$ is the two-dimensional multi-index of nonnegative integers α_i with degree $|\alpha| = \alpha_1 + \alpha_2 \leqslant \ell$ and such that $\mathbf{x}^\alpha = x_1^{\alpha_1} x_2^{\alpha_2}$ for any $\mathbf{x} \in \mathbb{R}^2$.

Finally, we use the symbols $\lesssim$ and $\gtrsim$ to denote inequalities holding up to a positive constant that is independent of the characteristic length of mesh elements, but may depend on the problem constants, like the coercivity and continuity constants, or other discretization constants like the mesh regularity constant, the stability constants, etc. Accordingly, $a \simeq b$ means $a \lesssim b \lesssim a$. The hidden constant generally has a different value at each occurrence.

2. Model problem and Virtual Element discretization

Let $\Omega \subset \mathbb{R}^2$ be a bounded polygonal domain. In this paper we are interested in deriving anisotropic error estimates for the virtual element approximation of the following elliptic problem:

$$-\Delta u = f \quad \text{in } \Omega, \qquad u = 0 \quad \text{on } \partial\Omega \tag{2.1}$$

with $f \in L^2(\Omega)$. The variational formulation of (2.1) reads as: Find $u \in H_0^1(\Omega)$ such that

$$a(u,v) = F(v) \tag{2.2}$$

for every $v \in H_0^1(\Omega)$ where $a(u,v) = \int_\Omega \nabla u \cdot \nabla v \, d\mathbf{x}$ and $F(v) = \int_\Omega f v \, d\mathbf{x}$.

We now briefly recall (see Beirão da Veiga *et al.* (2013) for more details) the lowest order virtual element approximation to (2.2). Let $\{\mathscr{K}_h\}_h$ be a sequence of decompositions of Ω where each mesh $\mathscr{K}_h$ is a collection of nonoverlapping polygonal elements K with boundary ∂K, and let $\mathscr{E}_h$ be the set of edges E of $\mathscr{K}_h$. Each mesh is labeled by h, the diameter of the mesh, defined as usual by $h = \max_{E\in\mathscr{K}_h} h_K$, where $h_K = \sup_{\mathbf{x},\mathbf{y}\in K} |\mathbf{x}-\mathbf{y}|$. We denote the set of vertices v in $\mathscr{K}_h$ by $\mathscr{V}_h$. The global lowest order virtual element space is defined as

$$V_{h,0} = \{v_h \in H_0^1(\Omega) : \ v_h|_K \in V_h^K \text{ and } v_h(\mathsf{v}) = 0 \ \forall \mathsf{v} \in \partial\Omega\} \subset H_0^1(\Omega), \tag{2.3}$$

where

$$V_h(K) = \{v_h \in H^1(K) : \ \Delta v_h = 0 \text{ in } K, \ v_h|_E \in \mathbb{P}^1(E) \ \forall E \subset \partial K\}, \tag{2.4}$$

is the local virtual element space. As usual (see, e.g., Beirão da Veiga *et al.* (2013)), we introduce the H^1 projector $\Pi^{\nabla,K} : V_h(K) \to \mathbb{P}_1(K)$. We denote by $u_h \in V_{h,0}$ the virtual element approximation to the solution u of (2.2), defined as the unique solution to

$$a_h(u_h, v_h) = (f_h, v_h) \tag{2.5}$$

for every $v_h \in V_{h,0}$, where f_h is the piecewise constant approximation of f on $\mathscr{K}_h$ and $a_h(u_h,v_h) = \sum_{K\in\mathscr{K}_h} a_h^K(u_h,v_h)$ being

$$a_h^K(u_h,v_h) = \int_K \nabla(\Pi^{\nabla,K}u_h)\cdot\nabla(\Pi^{\nabla,K}v_h)\, d\mathbf{x} + S^K((I-\Pi^{\nabla,K})u_h, (I-\Pi^{\nabla,K})v_h),$$

the local discrete bilinear form that satisfies the usual stability and consistency properties (see Beirão da Veiga *et al.* (2013) for precise definitions). For $w_h \in \mathrm{Ker}(\Pi^{\nabla,K})$ the stabilization form $S^K(\cdot,\cdot)$ is defined as

$$S^K(w_h,w_h) = \sum_{i=1}^{n_K} w_h^2(\mathsf{v}_{i,K}),$$

being $\mathsf{v}_{i,K}$, $i = 1,\dots,n_K$ the vertices of K. For more details about different choices for the stabilization form, see Beirão da Veiga *et al.* (2017).

3. Polygonal Anisotropy and mesh regularity

In this section, following Weisser (2019), we first make precise the notions of *isotropic* and *anisotropic* polygonal element. This will be obtained analysing the spectral decomposition of a suitable matrix (in the sequel named *covariance* matrix) associated to the element. More precisely, let K be a polygonal element of the partition $\mathscr{K}_h$. We denote by $|K|$ the area of K, we define the barycenter of K as

$$\bar{\mathbf{x}}_K = \frac{1}{|K|}\int_K \mathbf{x}\, d\mathbf{x},$$

and we introduce the covariance matrix of K as

$$M_{\mathrm{Cov}}(K) = \frac{1}{|K|}\int_K (\mathbf{x}-\bar{\mathbf{x}}_K)(\mathbf{x}-\bar{\mathbf{x}}_K)^\top \, d\mathbf{x} \in \mathbb{R}^{2\times 2}. \tag{3.1}$$

Obviously, M_{Cov} is real valued, symmetric and positive definite, once we assume that K is not degenerating (i.e. $|K| > 0$). Therefore, M_{Cov} admits an eigenvalue decomposition

$$M_{\mathrm{Cov}}(K) = U_K \Lambda_K U_K^\top,$$

with

$$U^\top = U^{-1} \quad \text{and} \quad \Lambda_K = \text{diag}\,(\lambda_{K,1}, \lambda_{K,2}), \tag{3.2}$$

where $\lambda_{K,1} \geqslant \lambda_{K,2} > 0$ only depend on the shape of K but not on its orientation.

The eigenvectors of $M_{\text{Cov}}(K)$ give the characteristic directions of K. Consequently, if

$$M_{\text{Cov}}(K) = cI$$

for $c > 0$, there are no dominant directions in the element K. Thus, we can characterise the anisotropy with the help of the quotient $\lambda_{K,1}/\lambda_{K,2} \geqslant 1$ and say that an element K is

$$\text{isotropic, if} \quad \frac{\lambda_{K,1}}{\lambda_{K,2}} \approx 1,$$
$$\text{and anisotropic, if} \quad \frac{\lambda_{K,1}}{\lambda_{K,2}} \gg 1.$$

Hinging upon the above spectral informations on the polygonal elements, we introduce a linear transformation of an anisotropic element K onto a kind of reference element $\widehat{K}$. For each $\mathbf{x} \in K$, we define the mapping by

$$\mathbf{x} \mapsto \widehat{\mathbf{x}} = F_K(\mathbf{x}) = A_K \mathbf{x} \quad \text{with} \quad A_K = \alpha_K \Lambda_K^{-1/2} U_K^\top \tag{3.3}$$

where $\alpha_K > 0$ will be chosen later. From now on, $\widehat{K} = F_K(K)$ will be called the reference element associated to K.

It is possible to prove (see Weisser (2019)) the following result.

LEMMA 3.1 There holds

1. $|\widehat{K}| = \alpha_K^2 |K| / \sqrt{\det(M_{\text{Cov}}(K))}$,
2. $\overline{\mathbf{x}}_{\widehat{K}} = F_K(\overline{\mathbf{x}}_K)$,
3. $M_{\text{Cov}}(\widehat{K}) = \alpha_K^2 I$.

According to the previous lemma, the reference element $\widehat{K}$ is isotropic, since $\lambda_{\widehat{K},1}/\lambda_{\widehat{K},2} = 1$, and thus, it has no dominant direction. For what concerns the choice of the parameter α_K we set

$$\alpha_K = \left(\frac{\sqrt{\det(M_{\text{Cov}}(K))}}{|K|} \right)^{1/d} = \left(\frac{\sqrt{\lambda_{K,1}\lambda_{K,2}}}{|K|} \right)^{1/2}, \tag{3.4}$$

which obviously ensures, in view of Lemma 3.1, $|\widehat{K}| = 1$.

In the sequel, we will work under the following assumption on the behaviour of the constant α_K.

Assumption 3.1. *We assume that it holds $\alpha_K \simeq 1$ for every $K \in \mathscr{K}_h$, uniformly in h.*

For a numerical exploration on the validity of Assumption 3.1 see (Weisser, 2019, Section 6.2). For future use, we note that the above assumption implies

$$|K| \simeq \sqrt{\lambda_{K,1}\lambda_{K,2}}. \tag{3.5}$$

As usual, we mark the operators and functions defined over the reference configuration by a hat, as, for instance,

$$\widehat{v} = v \circ F_K^{-1} : \widehat{K} \to K.$$

Obviously, it is

$$\nabla v = \alpha_K U_K \Lambda_K^{-1/2} \widehat{\nabla} \widehat{v}, \tag{3.6}$$

and, after some algebra,

$$\widehat{H}(\widehat{v}) = \alpha_K^{-2} \Lambda_K^{1/2} U_K^\top H(v) U_K \Lambda_K^{1/2}, \tag{3.7}$$

where $H(v)$ denotes the Hessian matrix of $v \in H^2(\Omega)$ and $\widehat{H}(\widehat{v})$ the corresponding Hessian on the reference configuration.

Following Weisser (2019), we are now ready to state the mesh requirements which will be needed in the sequel for deriving the properties of the quasi-interpolation operator (Section 4) and the anisotropic a posteriori error analysis (Section 5). We first recall the notion of isotropic regular polygonal meshes (Definition 3.3) which is instrumental for the definition of *anisotropic* polygonal meshes (Definition 3.4).

DEFINITION 3.2 (**regular isotropic element**) An element $K \in \mathscr{K}_h$ is said to be regular if

(a) K is a star-shaped polygon with respect to a circle of radius ρ_K and center $z_K \in K$.

(b) The aspect ratio is uniformly bounded from above by $\sigma_{\mathscr{K}}$, i.e. $h_K/\rho_K < \sigma_{\mathscr{K}}$, being h_K the diameter of K.

(c) For every edge $E \subset \partial K$ it holds $h_K \leqslant c_{\mathscr{K}} h_E$, being h_E the length of E.

DEFINITION 3.3 (**regular isotropic mesh**) A polygonal mesh $\mathscr{K}_h$ is called *regular* or a *regular isotropic mesh*, if all elements $K \in \mathscr{K}_h$ are regular in the sense of Definition 3.2 and the constants $\sigma_{\mathscr{K}}$ and $c_{\mathscr{K}}$ have to be uniformly bounded for all considered regular elements.

DEFINITION 3.4 (**regular anisotropic mesh**) Let $\mathscr{K}_h$ be a polygonal mesh with anisotropic elements. $\mathscr{K}_h$ is called *regular* or a *regular anisotropic mesh*, if

(a') The reference configuration $\widehat{K}$ for all $K \in \mathscr{K}_h$ obtained by (3.3) is a regular polygonal element according to Definition 3.2.

(b') Neighbouring elements behave similarly in their anisotropy. More precisely, for two neighbouring elements K^+ and K^-, i.e. $\overline{K^+} \cap \overline{K^-} \neq \varnothing$, with covariance matrices

$$M_{\mathrm{Cov}}(K^+) = U_{K^+} \Lambda_{K^+} U_{K^+}^\top \quad \text{and} \quad M_{\mathrm{Cov}}(K^-) = U_{K^-} \Lambda_{K^-} U_{K^-}^\top$$

as defined above, we can write

$$\Lambda_{K^-} = (I + \Delta^{K^+,K^-}) \Lambda_{K^+} \quad \text{with} \quad \Delta^{K^+,K^-} = \operatorname{diag}\left(\delta_1^{K^+,K^-}, \delta_2^{K^+,K^-}\right),$$

and

$$U_{K^-} = R^{K^+,K^-} U_{K^+} \quad \text{with} \quad R^{K^+,K^-} \text{ rotation matrix}$$

where for $i = 1, 2$

$$0 \leqslant |\delta_i^{K^+,K^-}| < c_\delta < 1 \quad \text{and} \quad \|I - R^{K^+,K^-}\|_0 \left(\frac{\lambda_{K^+,1}}{\lambda_{K^+,2}}\right)^{1/2} < c_\phi .$$

uniformly for all neighbouring elements, being $\|\cdot\|_0$ the spectral norm.

Thus a regular anisotropic element can be mapped according to (3.3) onto a regular polygonal element in the usual sense. In the definition of quasi-interpolation operators (see Section 4), we deal, however, with patches of elements instead of single elements. Thus, we study the mapping of such patches. Let $\omega = \omega_{\mathsf{v}}$ be the neighbourhood of the vertex v which is defined by

$$\overline{\omega}_{\mathsf{v}} = \bigcup \left\{ \overline{K'} : \mathsf{v} \in \overline{K'}, \quad K' \in \mathscr{K}_h \right\}.$$

Furthermore, for $K \in \mathscr{K}_h$, recall that the map F_K defined in (3.3) is given by

$$\mathbf{x} \mapsto F_K(\mathbf{x}) = A_K \mathbf{x} = \alpha_K \Lambda_K^{-1/2} U_K^\top \mathbf{x}.$$

Consequently, we may write $\widehat{K} = F_K(K)$ and we know, that $\widehat{K}$ is regular for all $K \in \mathscr{K}_h$ with some regularity parameters $\sigma_{\mathscr{K}}$ and $c_{\mathscr{K}}$. However, let now $K^+, K^- \in \mathscr{K}_h$ with $K^+, K^- \subset \omega$. We are interested in the regularity of $F_{K^+}(\omega)$ and $F_{K^+}(K^-)$. For the proofs of the following results we refer to Weisser (2019).

LEMMA 3.2 Let $\mathscr{K}_h$ be a regular anisotropic mesh, $\omega = \omega_{\mathsf{v}}$ be a patch as described above, and $K^+, K^- \in \mathscr{K}_h$ with $K^+, K^- \subset \omega$. The mapped element $F_{K^+}(K^-)$ is regular in the sense of Definition 3.3 with slightly perturbed regularity parameters $\widetilde{\sigma}_{\mathscr{K}}$ and $\widetilde{c}_{\mathscr{K}}$. Consequently, the mapped patch $F_K(\omega)$ consists of regular polygonal elements for all $K \in \mathscr{K}_h$ with $K \subset \omega$.

PROPOSITION 3.5 Let $\mathscr{K}_h$ be a regular anisotropic mesh. Each vertex v of the mesh $\mathscr{K}_h$ belongs to a uniformly bounded number of elements. Viceversa, each element $K \in \mathscr{K}_h$ has a uniformly bounded number of vertices on its boundary.

In the rest of the paper we will work under the following mesh assumption.

Assumption 3.6. *Let $\{\mathscr{K}_h\}_h$ be a sequence of regular anisotropic meshes with regularity parameters uniformly bounded with respect to h.*

Finally, we recall some instrumental results (see Weisser (2019) for the proofs) that will be employed in the next section.

LEMMA 3.3 Let $K \in \mathscr{K}_h$ be a polygonal element of a regular anisotropic mesh $\mathscr{K}_h$. Then, for $v \in H^1(K)$ and corresponding $\widehat{v} \in H^1(\widehat{K})$ there holds

$$\|\widehat{\nabla}\widehat{v}\|_{L^2(\widehat{K})} = |K|^{-1/2}\|A_K^{-T}\nabla v\|_{L^2(K)} \tag{3.8}$$

$$\sqrt{\frac{\lambda_{K,2}}{\lambda_{K,1}}}\,|\widehat{v}|^2_{H^1(\widehat{K})} \leqslant |v|^2_{H^1(K)} \leqslant \sqrt{\frac{\lambda_{K,1}}{\lambda_{K,2}}}\,|\widehat{v}|^2_{H^1(\widehat{K})}. \tag{3.9}$$

Moreover, under Assumption 3.1 there holds

$$\|\widehat{v}\|_{L^2(\widehat{K})} \simeq |K|^{-1/2}\|v\|_{L^2(K)}, \tag{3.10}$$

where the hidden constants are the ones appearing in (3.5).

LEMMA 3.4 (**anisotropic trace inequality**) Let $K \in \mathscr{K}_h$ be a polygonal element of a regular anisotropic mesh $\mathscr{K}_h$. For an edge $E \subset \partial K$ it holds

$$\|v\|^2_{L_2(E)} \lesssim \frac{|E|}{|K|}\left(\|v\|^2_{L_2(K)} + \|\alpha_K^{-1}\Lambda_K^{1/2}U_K^\top\nabla v\|^2_{L_2(K)}\right). \tag{3.11}$$

LEMMA 3.5 (**best-approximation by a constant**) Let $K \in \mathscr{K}_h$ be a polygonal element of a regular anisotropic mesh $\mathscr{K}_h$. For $v \in H^1(K)$, there exists a constant $p \in \mathscr{P}^0(K)$ such that

$$\|v - p\|_{L_2(K)} \lesssim \|\alpha_K^{-1}\Lambda_K^{1/2}U_K^\top\nabla v\|_{L_2(K)}.$$

4. Quasi-Interpolation of Functions in $H^1(\Omega)$

Let ω be a patch of physical elements belonging to a regular anisotropic polygonal mesh. Let $\widehat{\omega}$ be the patch of reference elements $\widehat{K}$ such that $\widehat{\omega} = F_{K^*}(\omega)$, where the mapping is dictated by an element K^* of the patch ω (i.e. all the elements of the patch ω are transformed based on employing the same map F_K, where K is one of the elements of the patch). On the reference patch $\widehat{\omega}$ we introduce the space

$$\widehat{\Theta}(\widehat{\omega}) = \{\widehat{\theta} \in C^0(\widehat{\omega}) :\ \forall \widehat{K} \in \widehat{\omega}\ \widehat{\theta}_{|\widehat{K}} = \theta \circ F_{K^*}^{-1},\ \theta \in V_h(F_{K^*}^{-1}(\widehat{K}))\} \tag{4.1}$$

where $V_h(F_{K^*}^{-1}(\widehat{K}))$ is the lowest order local virtual element space defined on the polygon $F_{K^*}^{-1}(\widehat{K})$.[1] We remark that in view of Lemma 3.2 the specific choice of the element K^* in the definition of the space $\widehat{\Theta}(\widehat{\omega})$ is not restrictive. Moreover, we observe that, in view of Assumption 3.6, the dimension of $\widehat{\Theta}(\widehat{\omega})$ is uniformly bounded with respect to h. Finally, it is worth noticing that functions in $\widehat{\Theta}(\widehat{\omega})$ are not necessarily virtual element functions. However, constant functions are contained in $\widehat{\Theta}(\widehat{\omega})$ and this will be sufficient for our scopes.

Now, following Bernardi & Girault (1998), we introduce a projection operator $\widehat{r}_\omega(\widehat{v})$ on the reference patch $\widehat{\omega}$.

DEFINITION 4.1 For any function $\widehat{v} \in L^1(\widehat{\omega})$ we define $\widehat{r}_\omega(\widehat{v}) \in \widehat{\Theta}(\widehat{\omega})$ as

$$\int_{\widehat{\omega}} (\widehat{r}_{\widehat{\omega}}(\widehat{v}) - \widehat{v})\widehat{\theta} = 0 \qquad \forall \widehat{\theta} \in \widehat{\Theta}(\widehat{\omega}). \tag{4.2}$$

[1] Note that the polygon $F_{K^*}^{-1}(\widehat{K})$ is not necessarily equal to K^*, unless we consider exactly the reference polygon $\widehat{K^*}$ associated to K^*.

It is important to remark that $\widehat{r}_{\widehat{\omega}}$ is a projection operator on $\widehat{\omega}$.

On the physical patch ω we can define $r_\omega(v)$ so that $r_\omega(v)\circ F_{K^*}^{-1} = \widehat{r}_{\widehat{\omega}}(v\circ F_{K^*}^{-1})$, i.e. $\widehat{r_\omega(v)} = \widehat{r}_{\widehat{\omega}}(\widehat{v})$. Let ω_i be the patch of elements sharing the vertex v_i and set $r_i = r_{\omega_i}$. The operators r_i will be employed to build the quasi-interpolant $\mathfrak{I}_C$ (see (4.7) below). In the sequel, we collect some approximation results for r_i that will be instrumental for proving the approximation properties of $\mathfrak{I}_C$.

LEMMA 4.1 Let $\mathscr{K}_h$ be a *regular anisotropic mesh*. For any $K\subset\omega_i$ there hold

$$\|u-r_i(u)\|^2_{L^2(K)} \lesssim \sum_{\widetilde{K}\subset\omega_i}\frac{|K|}{|\widetilde{K}|}\|A_{\widetilde{K}}^{-T}\nabla u\|^2_{L^2(\widetilde{K})}. \tag{4.3}$$

which can also be written in the following way

$$\|u-r_i(u)\|^2_{L^2(K)} \lesssim |K|\sum_{\widetilde{K}\subset\omega_i}\sqrt{\frac{\lambda_{\widetilde{K},1}}{\lambda_{\widetilde{K},2}}}|u|^2_{H^1(\widetilde{K})}. \tag{4.4}$$

Proof. Let $K\in\omega_i$ then we have

$$\|u-r_i(u)\|_{L^2(K)} \lesssim |K|^{1/2}\|\widehat{u}-\widehat{r}_{\widehat{\omega}_i}(\widehat{u})\|_{L^2(\widehat{K})}. \tag{4.5}$$

Now, employing the fact that $\widehat{r}_{\widehat{\omega}_i}$ is a projector on $\widehat{\omega}_i$ we have

$$\widehat{u}-\widehat{r}_{\widehat{\omega}_i}(\widehat{u}) = \widehat{u}-\widehat{\theta}-\widehat{r}_{\widehat{\omega}_i}(\widehat{u}-\widehat{\theta}),$$

for $\widehat{\theta}\in\widehat{\Theta}(\widehat{\omega}_i)$ which implies

$$\|\widehat{u}-\widehat{r}_{\widehat{\omega}_i}(\widehat{u})\|_{L^2(\widehat{\omega}_i)} \leqslant 2\|\widehat{u}-\widehat{\theta}\|_{L^2(\widehat{\omega}_i)}.$$

Assume $\widehat{\theta}$ is constant on $\widehat{\omega}_i$ and $\widehat{u}\in H^1(\widehat{\omega}_i)$, hence employing standard interpolation error estimate together with (3.8) we have

$$\begin{aligned}
\|\widehat{u}-\widehat{r}_{\widehat{\omega}_i}(\widehat{u})\|_{L^2(\widehat{\omega}_i)} &\lesssim |\widehat{u}|_{H^1(\widehat{\omega}_i)}\\
&\lesssim \left(\sum_{\widehat{K}\subset\widehat{\omega}_i}|\widehat{u}|^2_{H^1(\widehat{K})}\right)^{1/2}\\
&\lesssim \left(\sum_{\widetilde{K}\subset\omega_i}|\widetilde{K}|^{-1}\|A_{\widetilde{K}}^{-T}\nabla u\|^2_{L^2(\widetilde{K})}\right)^{1/2}.
\end{aligned}$$

Combining (4.5) with the above inequality yields (4.3). On the other hand, using (3.8)-(3.9) we get (4.4). □

LEMMA 4.2 For any $K\subset\omega_i$ there holds

$$|u-r_i(u)|^2_{H^1(K)} \lesssim \sum_{\widetilde{K}\subset\omega_i}\sqrt{\frac{\lambda_{K,1}\lambda_{\widetilde{K},1}}{\lambda_{K,2}\lambda_{\widetilde{K},2}}}|u|^2_{H^1(\widetilde{K})}. \tag{4.6}$$

Proof. By using (3.9) and taking $\widehat{\theta}$ constant on $\widehat{\omega}_i$, employing the equivalence of all norms on the finite dimensional space $\widehat{\Theta}(\widehat{\omega}_i)$ (see Proposition A.1 below), the fact that $\widehat{r}_{\widehat{\omega}_i}$ is a projection on $\widehat{\omega}_i$ and standard

interpolation error estimate we obtain

$$\begin{aligned}
|u-r_i(u)|_{H^1(K)} &\leqslant \left(\frac{\lambda_{K,1}}{\lambda_{K,2}}\right)^{1/4} |\widehat{u}-\widehat{r}_{\widehat{\omega}_i}(\widehat{u})|_{H^1(\widehat{K})} \leqslant \left(\frac{\lambda_{K,1}}{\lambda_{K,2}}\right)^{1/4} |\widehat{u}-\widehat{r}_{\widehat{\omega}_i}(\widehat{u})|_{H^1(\widehat{\omega}_i)} \\
&\leqslant \left(\frac{\lambda_{K,1}}{\lambda_{K,2}}\right)^{1/4} \left(|\widehat{u}-\widehat{\theta}|_{H^1(\widehat{\omega}_i)} + |\widehat{\theta}-\widehat{r}_{\widehat{\omega}_i}(\widehat{u})|_{H^1(\widehat{\omega}_i)}\right) \\
&\lesssim \left(\frac{\lambda_{K,1}}{\lambda_{K,2}}\right)^{1/4} \left(|\widehat{u}-\widehat{\theta}|_{H^1(\widehat{\omega}_i)} + \|\widehat{\theta}-\widehat{r}_{\widehat{\omega}_i}(\widehat{u})\|_{L^2(\widehat{\omega}_i)}\right) \\
&\lesssim \left(\frac{\lambda_{K,1}}{\lambda_{K,2}}\right)^{1/4} \left(|\widehat{u}-\widehat{\theta}|_{H^1(\widehat{\omega}_i)} + \|\widehat{r}_{\widehat{\omega}_i}(\widehat{\theta}-\widehat{u})\|_{L^2(\widehat{\omega}_i)}\right) \\
&\lesssim \left(\frac{\lambda_{K,1}}{\lambda_{K,2}}\right)^{1/4} \left(|\widehat{u}-\widehat{\theta}|_{H^1(\widehat{\omega}_i)} + \|\widehat{\theta}-\widehat{u}\|_{L^2(\widehat{\omega}_i)}\right) \\
&\lesssim \left(\frac{\lambda_{K,1}}{\lambda_{K,2}}\right)^{1/4} |\widehat{u}|_{H^1(\widehat{\omega}_i)}.
\end{aligned}$$

Note that if $\hat{u}|_{\hat{\omega}_i}$ is constant we take $\widehat{\theta} = \widehat{u}|_{\widehat{\omega}_i}$, whereas if $\widehat{r}_{\widehat{\omega}_i}(\widehat{u})$ is constant (and $\hat{u}|_{\hat{\omega}_i}$ is not constant) we take $\hat{\theta} = \widehat{r}_{\widehat{\omega}_i}(\widehat{u})$. By using (3.9) on each $\widehat{K} \subset \widehat{\omega}_i$ we get the thesis. □

We are now ready to introduce the quasi-interpolation operator. For simplicity of exposition, we first consider the case where no boundary conditions are imposed on the boundary of Ω. To this aim, we introduce the global lowest order virtual element space $V_h \subset H^1(\Omega)$, which is defined as $V_{h,0}$ except for the conditions imposed on the boundary vertexes (cf. (2.3)). The quasi-interpolation of lowest order $\mathfrak{I}_C : H^1(\Omega) \to V_h$ is defined as

$$(\mathfrak{I}_C v)(x) = \sum_{i=1}^{N} [r_i(v)](\mathsf{v}_i)\, \varphi_i(x) \tag{4.7}$$

where $r_i = r_{\omega_i}$ and $\varphi_i \in V_h$ is the global virtual element basis function with $\varphi_i(\mathsf{v}_j) = \delta_{i,j}$, $i,j = 1,\dots,N$.

We first observe that under Assumption 3.1 and employing a generalized scaling argument it is possible to derive the following anisotropic inverse inequality (cf. Beirão da Veiga *et al.* (2017); Chen & Huang (2018); Vacca (2018) for the isotropic case).

LEMMA 4.3 Under Assumption 3.1, for any $v \in V_h(K)$ there holds

$$|v|_{H^1(K)} \lesssim \frac{1}{\sqrt{\lambda_{K,2}}} \|v\|_{L^2(K)}. \tag{4.8}$$

Proof. We first observe that the equivalence of all norms on finite dimensional spaces (cf. Proposition A.1 below) implies

$$|\hat{v}|_{H^1(\hat{K})} \lesssim \|\hat{v}\|_{L^2(\hat{K})}.$$

Employing (3.9) and (3.10) yields the thesis. □

REMARK 4.1 On the rectangle $K = (0,a)\times(0,b)$, with $a > b$, we consider, for instance, the local virtual element basis functions $\varphi(x,y) = \frac{xy}{ab}$. We observe that $\lambda_{K,1} = \frac{a^2}{12}$ and $\lambda_{K,2} = \frac{b^2}{12}$. Straightforward computations yield $\|\nabla\varphi\|^2_{L^2(K)} = \frac{a^2+b^2}{3ab}$ and $\|\varphi\|^2_{L^2(K)} = \frac{ab}{9}$. Hence, we get

$$\|\nabla\varphi\|_{L^2(K)} \lesssim \frac{1}{b}\|\varphi\|_{L^2(K)} \lesssim \frac{1}{\sqrt{\lambda_{K,2}}}\|\varphi\|_{L^2(K)}.$$

THEOREM 4.2 For any $K \subset \mathscr{K}_h$ there hold

$$\|u-\mathfrak{I}_C u\|^2_{L^2(K)} \lesssim \sum_{i=1}^{n_K} \sum_{\widetilde{K}\subset\omega_i} \frac{|K|}{|\widetilde{K}|} \|A_{\widetilde{K}}^{-T}\nabla u\|^2_{L^2(\widetilde{K})}, \tag{4.9}$$

or, written in an alternative way,

$$\|u-\mathfrak{I}_C u\|^2_{L^2(K)} \lesssim |K| \sum_{i=1}^{n_K} \sum_{\widetilde{K}\subset\omega_i} \sqrt{\frac{\lambda_{\widetilde{K},1}}{\lambda_{\widetilde{K},2}}} |u|^2_{H^1(\widetilde{K})}, \tag{4.10}$$

where n_K denotes the number of vertices of K.

Proof. Denoting by n_K the number of vertices of K and by ω_i the patch of elements sharing the i-th vertex of K we have

$$\begin{aligned}(u-\mathfrak{I}_C u)|_K &= u|_K - \sum_{i=1}^{n_K}[r_1(u)](\mathsf{v}_i)\varphi_i|_K - \sum_{i=2}^{n_K}[r_i(u)-r_1(u)](\mathsf{v}_i)\varphi_i|_K \\ &= (u-r_1(u))|_K - \sum_{i=2}^{n_K}[r_i(u)-r_1(u)](\mathsf{v}_i)\varphi_i|_K,\end{aligned}$$

where in the last step we employed the fact that $r_1(u)$ is a virtual element function defined on the patch $F_K^{-1}(\widehat{\omega})$ and $K \subset F_K^{-1}(\widehat{\omega})$. It follows

$$\begin{aligned}\|u-\mathfrak{I}_C u\|_{L^2(K)} &\leqslant \|u-r_1(u)\|_{L^2(K)} + \sum_{i=2}^{n_K}|[r_i(u)-r_1(u)](\mathsf{v}_i)|\|\varphi_i\|_{L^2(K)} \\ &\leqslant \|u-r_1(u)\|_{L^2(K)} + |K|^{1/2}\sum_{i=2}^{n_K}\|r_i(u)-r_1(u)\|_{L^\infty(K)}.\end{aligned}$$

To conclude, it is enough to employ Lemma 4.1 in combination with the following bound

$$\begin{aligned}\|r_i(u)-r_1(u)\|_{L^\infty(K)} &= \|\widehat{r}_i(\widehat{u})-\widehat{r}_1(\widehat{u})\|_{L^\infty(\widehat{K})} \\ &\lesssim \|\widehat{r}_i(\widehat{u})-\widehat{r}_1(\widehat{u})\|_{L^2(\widehat{K})} \lesssim \|\widehat{u}-\widehat{r}_i(\widehat{u})\|_{L^2(\widehat{K})} + \|\widehat{u}-\widehat{r}_1(\widehat{u})\|_{L^2(\widehat{K})} \\ &\lesssim |K|^{-1/2}\left(\|u-r_i(u)\|_{L^2(K)} + \|u-r_1(u)\|_{L^2(K)}\right), \qquad (4.11)\end{aligned}$$

where in the first inequality we employed the fact that all norms are equivalent on the finite dimensional space $\widehat{\Theta}(\widehat{\omega})$ (cf. Proposition A.1 below). □

COROLLARY 4.1 There holds

$$\|u-\mathfrak{I}_C u\|^2_{L^2(K)} \lesssim \sum_{i=1}^{n_K}\sum_{\widetilde{K}\subset\omega_i}\|A_{\widetilde{K}}^{-T}\nabla u\|^2_{L^2(\widetilde{K})}, \qquad (4.12)$$

where n_K denotes the number of vertices of K.

Proof. Thanks to the mesh regularity assumption it is possible to prove that $\frac{|K|}{|\widetilde{K}|}$ is bounded. □

THEOREM 4.3 Under Assumption 3.1, for any $K \subset \omega_i$ there holds

$$|u-\mathfrak{I}_C u|_{H^1(K)} \lesssim \left(\frac{\lambda_{K,1}}{\lambda_{K,2}}\right)^{1/2}|u|_{H^1(\omega_K)}, \qquad (4.13)$$

ω_K being the patch of polygons K' such that $\overline{K'}\cap\overline{K}\neq\emptyset$.

Proof. Following the proof of Theorem 4.2 and employing Lemma 4.2 we have

$$\begin{aligned}|u-\mathfrak{I}_C u|_{H^1(K)} &\leqslant |u-r_1(u)|_{H^1(K)} + \sum_{i=2}^{n_K}|[r_i(u)-r_1(u)](\mathsf{v}_i)||\varphi_i|_{H^1(K)} \\ &\leqslant \left(\sum_{\widetilde{K}\subset\omega_1}\sqrt{\frac{\lambda_{K,1}\lambda_{\widetilde{K},1}}{\lambda_{K,2}\lambda_{\widetilde{K},2}}}|u|^2_{H^1(\widetilde{K})}\right)^{1/2} + \sum_{i=2}^{n_K}|[r_i(u)-r_1(u)](\mathsf{v}_i)||\varphi_i|_{H^1(K)}.\end{aligned}$$

Now, we observe that, similarly to the proof of Theorem 4.2, employing (3.10) together with Lemma 4.1 the following holds

$$\begin{aligned}\|r_i(u)-r_1(u)\|_{L^\infty(K)} &= \|\widehat{r}_i(\widehat{u})-\widehat{r}_1(\widehat{u})\|_{L^\infty(\widehat{K})} \\ &\lesssim |\widehat{r}_i(\widehat{u})-\widehat{r}_1(\widehat{u})|_{L^2(\widehat{K})} \lesssim |\widehat{u}-\widehat{r}_i(\widehat{u})|_{L^2(\widehat{K})} + |\widehat{u}-\widehat{r}_1(\widehat{u})|_{L^2(\widehat{K})} \\ &\lesssim |K|^{1/2}\left(|u-r_i(u)|_{L^2(K)} + |u-r_1(u)|_{L^2(K)}\right) \\ &\lesssim \left(\sum_{\widetilde{K}\subset\omega_1\cup\omega_i}\sqrt{\frac{\lambda_{\widetilde{K},1}}{\lambda_{\widetilde{K},2}}}|u|^2_{H^1(\widetilde{K})}\right)^{1/2}.\end{aligned}$$

Employing Lemma 4.3 and the fact that $\|\varphi\|_{L^2(K)} \leqslant |K|^{1/2}$ we have, after invoking Assumption 3.1 (see (3.5)), $|\varphi_i|_{H^1(K)} \lesssim \left(\frac{\lambda_{K,1}}{\lambda_{K,2}}\right)^{1/4}$. Thus, we get

$$\sum_{i=2}^{n_K} |[r_i(u) - r_1(u)](\mathsf{v}_i)||\varphi_i|_{H^1(K)} \lesssim \left(\frac{\lambda_{K,1}}{\lambda_{K,2}}\right)^{1/4} \sum_{i=1}^{n_K} \left(\sum_{\widetilde{K}\subset\omega_i} \sqrt{\frac{\lambda_{\widetilde{K},1}}{\lambda_{\widetilde{K},2}}} |u|^2_{H^1(\widetilde{K})} \right)^{1/2}.$$

As a consequence of the anisotropic mesh regularity assumption we have

$$\lambda_{K,i} \simeq \lambda_{\widetilde{K},i},\ i = 1,2$$

which yields

$$\sum_{i=2}^{n_K} |[r_i(u) - r_1(u)](\mathsf{v}_i)||\varphi_i|_{H^1(K)} \leqslant \left(\frac{\lambda_{K,1}}{\lambda_{K,2}}\right)^{1/2} |u|_{H^1(\omega_K)}.$$

Combining the above inequalities we obtain the thesis.

□

THEOREM 4.4 Let $E \subset \partial K$ be an edge of $K \in \mathscr{K}_h$. Then it holds

$$\|u - \mathfrak{I}_C u\|_{L^2(E)} \lesssim \frac{|E|^{1/2}}{|K|^{1/2}} \|A_{\widetilde{K}}^{-T} \nabla u\|_{L^2(\omega_E)} \tag{4.14}$$

being ω_E the patch of elements $\widetilde{K}$ having non-empty intersect with $\overline{E}$.

Proof. Let $E \subset \partial K$ be an edge of $K \in \mathscr{K}_h$ with endpoints v_1 and v_2. Observing that $r_1(u)$ is a virtual element function, we have

$$\begin{aligned} \|u - \mathfrak{I}_C u\|_{L^2(E)} &= \|u - \sum_{i=1}^{2} [r_i(u)](\mathsf{v}_i)\varphi_i\|_{L^2(E)} \\ &= \|u - r_1(u) - [r_2(u) - r_1(u)](\mathsf{v}_2)\varphi_2\|_{L^2(E)} \\ &\leqslant \|u - r_1(u)\|_{L^2(E)} + \|r_2(u) - r_1(u)\|_{L^\infty(E)} \|\varphi_2\|_{L^2(E)}. \end{aligned}$$

Noting that $\|\varphi_2\|_{L^2(E)} \leqslant |E|^{1/2}$, employing the norm equivalence on finite dimensional spaces and adapting the proof of Proposition A.1 below, it holds $\|r_2(u) - r_1(u)\|_{L^\infty(E)} = \|\widehat{r}_2(\widehat{u}) - \widehat{r}_1(\widehat{u})\|_{L^\infty(\widehat{E})} \lesssim \|\widehat{r}_2(\widehat{u}) - \widehat{r}_1(\widehat{u})\|_{L^2(\widehat{E})} \lesssim |E|^{-1/2} \|r_2(u) - r_1(u)\|_{L^2(E)}$ we have

$$\begin{aligned} \|u - \mathfrak{I}_C u\|_{L^2(E)} &\lesssim \|u - r_1(u)\|_{L^2(E)} + \|r_2(u) - r_1(u)\|_{L^2(E)} \\ &\lesssim \left(\frac{|E|}{|K|}\right)^{1/2} \Big(\|u - r_1(u)\|_{L^2(K)} + \|r_2(u) - r_1(u)\|_{L^2(K)} \\ &\quad + \|A_K^{-T} \nabla (u - r_1(u))\|_{L^2(K)} + \|A_K^{-T} \nabla (r_2(u) - r_1(u))\|_{L^2(K)} \Big), \end{aligned}$$

where we employed trace inequality (3.11). Now, using (4.3) and (3.8) we obtain

$$\begin{aligned} \|u - \mathfrak{I}_C u\|_{L^2(E)} &\lesssim \left(\frac{|E|}{|K|}\right)^{1/2} \Bigg(\left(\sum_{\widetilde{K}\subset\omega_1\cup\omega_2} \frac{|K|}{|\widetilde{K}|} \|A_{\widetilde{K}}^{-T} \nabla u\|^2_{L^2(\widetilde{K})} \right)^{1/2} \\ &\quad + |K|^{1/2} (\|\widehat{\nabla}(\widehat{u} - \widehat{r}_1(\widehat{u}))\|_{L^2(\widehat{K})} + \|\widehat{\nabla}(\widehat{u} - \widehat{r}_2(\widehat{u}))\|_{L^2(\widehat{K})}) \Bigg). \end{aligned}$$

Proceeding as in the proof of Lemma 4.2 and employing (3.8) we get for $i = 1,2$

$$\|\widehat{\nabla}(\widehat{u} - \widehat{r}_i(\widehat{u}))\|_{L^2(\widehat{K})} \lesssim |\widehat{u}|_{H^1(\widehat{\omega})} \lesssim \left(\sum_{\widetilde{K}\subset\omega_i} |\widetilde{K}|^{-1} \|A_{\widetilde{K}}^{-T} \nabla u\|^2_{L^2(\widetilde{K})} \right)^{1/2}.$$

Combining the above estimates and employing the anisotropic mesh assumptions guaranteeing $|K| \simeq |\widetilde{K}|$ for $K, \widetilde{K}$ belonging to the same patch, we obtain the thesis. □

In the following, we rewrite (4.12) and (4.14) in an equivalent way, suitable for future use when deriving in the next section polygonal anisotropic error estimates. More precisely, let $\mathbf{r}_{K,i}$ be the normalized eigenvectors to the eigenvalues $\lambda_{K,i}$ for $i = 1,2$, which have been used already several times in the matrix U_K. Namely, it is $U_K = (\mathbf{r}_{K,1}, \mathbf{r}_{K,2})$. Thus, we observe

$$\Lambda_K^{1/2} U_K^\top \nabla v = \begin{pmatrix} \lambda_{K,1}^{1/2}\, \mathbf{r}_{K,1} \cdot \nabla v \\ \lambda_{K,2}^{1/2}\, \mathbf{r}_{K,2} \cdot \nabla v \end{pmatrix},$$

and consequently

$$\|\alpha_K^{-1} \Lambda_K^{1/2} U_K^\top \nabla v\|^2_{L_2(\omega_K)} = \alpha_K^{-2} \left(\lambda_{K,1} \|\mathbf{r}_{K,1} \cdot \nabla v\|^2_{L_2(\omega_K)} + \lambda_{K,2} \|\mathbf{r}_{K,2} \cdot \nabla v\|^2_{L_2(\omega_K)} \right).$$

Furthermore, since $\mathbf{r}_{K,i} \cdot \nabla v \in \mathbb{R}$, we get

$$\begin{aligned} \|\mathbf{r}_{K,i} \cdot \nabla v\|^2_{L_2(\omega_K)} &= \sum_{K' \subset \omega_K} \int_{K'} (\mathbf{r}_{K,i}^\top \nabla v)^2 \, d\mathbf{x} \\ &= \sum_{K' \subset \omega_K} \int_{K'} \mathbf{r}_{K,i}^\top \nabla v (\nabla v)^\top \mathbf{r}_{K,i} \, d\mathbf{x} \\ &= \mathbf{r}_{K,i}^\top G_K(v)\, \mathbf{r}_{K,i}, \end{aligned}$$

with

$$G_K(v) = \sum_{K' \subset \omega_K} \begin{pmatrix} \|v_{x_1}\|^2_{L_2(K')} & \displaystyle\int_{K'} v_{x_1} v_{x_2} \, d\mathbf{x} \\ \displaystyle\int_{K'} v_{x_1} v_{x_2} \, d\mathbf{x} & \|v_{x_2}\|^2_{L_2(K')} \end{pmatrix}$$

where v_{x_i} stands for $\partial v / \partial x_i$. Thus (4.12) and (4.14) can be rewritten as

$$\|v - \mathfrak{I}_C v\|_{L_2(K)} \leqslant c\, \alpha_K^{-1} \left(\lambda_{K,1}\, \mathbf{r}_{K,1}^\top G_K(v)\, \mathbf{r}_{K,1} + \lambda_{K,2}\, \mathbf{r}_{K,2}^\top G_K(v)\, \mathbf{r}_{K,2} \right)^{1/2} \tag{4.15}$$

and

$$\|v - \mathfrak{I}_C v\|_{L_2(E)} \leqslant c\, \alpha_K^{-1}\, \frac{|E|^{1/2}}{|K|^{1/2}} \left(\lambda_{K,1}\, \mathbf{r}_{K,1}^\top G_K(v)\, \mathbf{r}_{K,1} + \lambda_{K,2}\, \mathbf{r}_{K,2}^\top G_K(v)\, \mathbf{r}_{K,2} \right)^{1/2}, \tag{4.16}$$

respectively (cf. (Formaggia & Perotto, 2003, (2.12) and (2.15))).

We now introduce a variant of $\mathfrak{I}_C$ preserving the homogeneous boundary conditions. To this aim we number the N vertices of the partition so that the first N^∂ vertices are the boundary ones, while the remaining ones (i.e. from $N^\partial + 1$ to N) are the internal vertices. The quasi-interpolant $\mathfrak{I}_{C,0} : H_0^1(\Omega) \to V_{h,0}$ is thus defined as

$$\mathfrak{I}_{C,0} u = \sum_{i=N^\partial+1}^{N} [r_i(u)](\mathsf{v}_i)\, \varphi_i(x). \tag{4.17}$$

The results contained in Theorem 4.2, 4.3 and 4.4 are still true, and the analogous estimates to (4.15) and (4.16) hold as well. For instance, in order to extend Theorem 4.2 it is sufficient to observe that for $u \in H_0^1(\Omega)$ the following holds true

$$\|u - \mathfrak{I}_{C,0} u\|_{L^2(K)} \leqslant \|u - \mathfrak{I}_C u\|_{L^2(K)} + \sum_{i=1}^{N^\partial} |[r_i(u)](\mathsf{v}_i)|\, \|\varphi_i(x)\|_{L^2(K)}. \tag{4.18}$$

Finally, denoting by $E \subset \partial\Omega$ one of the two boundary edges containing the vertex v_i, employing the norm equivalence on finite dimensional spaces and adapting the proof of Proposition A.1, and observing $u|_{\partial\Omega} = 0$ we have

$$\begin{aligned} |[r_i(u)](\mathsf{v}_i)| &\leqslant \|r_i(u)\|_{L^\infty(E)} = \|\widehat{r}_i(\widehat{u})\|_{L^\infty(\widehat{E})} \lesssim \|\widehat{r}_i(\widehat{u})\|_{L^2(\widehat{E})} \\ &= \|\widehat{r}_i(\widehat{u}) - \widehat{u}\|_{L^2(\widehat{E})} \lesssim \|\widehat{r}_i(\widehat{u}) - \widehat{u}\|_{L^2(\widehat{K})} + |\widehat{r}_i(\widehat{u}) - \widehat{u}|_{H^1(\widehat{K})}, \end{aligned}$$

where in the last step we used standard trace inequality on regular isotropic elements. Finally, recalling that it holds

$$\|\widehat{r}_i(\widehat{u}) - \widehat{u}\|_{L^2(\widehat{K})} + |\widehat{r}_i(\widehat{u}) - \widehat{u}|_{H^1(\widehat{K})} \lesssim |\widehat{u}|_{H^1(\widehat{K})},$$

the analogous to Theorem 4.2 follows after employing (3.8) and summing over the boundary vertices.

5. Anisotropic a posteriori error estimate

In this section we derive an anisotropic polygonal a posteriori error estimate for the virtual element approximation of (2.1). We preliminary observe that in view of Lemma 3.3 the stabilization form satisfies

$$\sqrt{\frac{\lambda_{K,2}}{\lambda_{K,1}}}\, S^K(w_h, w_h) \lesssim |w_h|^2_{H^1(K)} \lesssim \sqrt{\frac{\lambda_{K,1}}{\lambda_{K,2}}}\, S^K(w_h, w_h), \tag{5.1}$$

for $w_h = (I - \Pi^{\nabla,K})v_h$, $v_h \in V_h(K)$. Indeed, it is sufficient to employ (3.9) in combination with the following

$$S^K(w_h, w_h) \simeq \|w_h\|^2_{L^\infty(K)} = \|\widehat{w}_h\|^2_{L^\infty(\widehat{K})} \simeq \|\widehat{w}_h\|^2_{H^1(\widehat{K})},$$

where we used the definition of S^K, the mesh assumption (in particular the uniform boundedness of the number n_K of element vertices) and the fact that on finite dimensional spaces all norms are equivalent.

REMARK 5.1 Let us comment on the bounds in (5.1). On the rectangle $K^* = (0,a) \times (0,b)$, with $a > b$, it can be easily seen that the virtual element basis functions in V_h are

$$\varphi_0(x,y) = \frac{xy}{ab} - \frac{y}{b} - \frac{x}{a} + 1, \qquad \varphi_1(x,y) = \frac{x}{a} - \frac{xy}{ab},$$
$$\varphi_2(x,y) = \frac{xy}{ab}, \qquad \varphi_3(x,y) = \frac{y}{b} - \frac{xy}{ab},$$

and, for $w_h = (I - \Pi^{\nabla,K})\varphi_i$, $i = 0, \dots, 3$, the following holds:

$$\lambda_{K,1} = \frac{a^2}{12}, \quad \lambda_{K,2} = \frac{b^2}{12},$$
$$\frac{|w_h|^2_{H^1(K^*)}}{S^{K^*}(w_h, w_h)} = \frac{1}{3}\left(\sqrt{\frac{\lambda_{K,1}}{\lambda_{K,2}}} + \sqrt{\frac{\lambda_{K,2}}{\lambda_{K,1}}}\right),$$

and hence

$$\frac{2}{3}\sqrt{\frac{\lambda_{K,2}}{\lambda_{K,1}}}\, S^{K^*}(w_h, w_h) \leqslant |w_h|^2_{H^1(K^*)} \leqslant \frac{2}{3}\sqrt{\frac{\lambda_{K,1}}{\lambda_{K,2}}}\, S^{K^*}(w_h, w_h).$$

We now state the main result of the paper.

PROPOSITION 5.1 Let $u_h \in V_{h,0}$ be the VEM approximation to the solution u of (2.1). Under Assumptions 3.6 and 3.1, for $e = u - u_h$ it holds

$$\begin{aligned}
\|\nabla e\|^2_{L^2(\Omega)} \lesssim\ & \sum_{K \in \mathscr{T}_h} \|R_K\|_{L^2(K)} \alpha_K^{-1} \left(\lambda_{K,1}\, \mathbf{r}^\top_{K,1} G_K(e)\, \mathbf{r}_{K,1} + \lambda_{K,2}\, \mathbf{r}^\top_{K,2} G_K(e)\, \mathbf{r}_{K,2}\right)^{1/2} \\
&+ \sum_{E \in \mathscr{S}_h} \|J_E\|_{L^2(E)} \alpha_K^{-1} \left(\frac{|E|}{|K|}\right)^{1/2} \left(\lambda_{K,1}\, \mathbf{r}^\top_{K,1} G_K(e)\, \mathbf{r}_{K,1} + \lambda_{K,2}\, \mathbf{r}^\top_{K,2} G_K(e)\, \mathbf{r}_{K,2}\right)^{1/2} \\
&+ \sum_{K \in \mathscr{T}_h} M_K^2 S^K((I - \Pi^{\nabla,K})u_h, (I - \Pi^{\nabla,K})u_h) \\
&+ \sum_{K \in \mathscr{T}_h} \|f - f_h\|_{L^2(K)} \alpha_K^{-1} \left(\lambda_{K,1}\, \mathbf{r}^\top_{K,1} G_K(e)\, \mathbf{r}_{K,1} + \lambda_{K,2}\, \mathbf{r}^\top_{K,2} G_K(e)\, \mathbf{r}_{K,2}\right)^{1/2},
\end{aligned}$$

where

$$\begin{aligned}
R_K &= f_h|_K, \\
J_E &= [\![\nabla(\Pi^{\nabla,K})u_h]\!]_E, \\
M_K &= \left(\frac{\lambda_{K,1}}{\lambda_{K,2}}\right)^{\frac{3}{4}}.
\end{aligned}$$

Proof. The proof closely follows Cangiani *et al.* (2017b). Let us set $e = u - u_h \in H^1_0(\Omega)$ and we preliminary observe that for every $v \in H^1_0(\Omega)$ the following holds

$$\begin{aligned} a(e,v) &= (f,v) - a(u_h,\chi) - a(u_h, v-\chi) \\ &= (f-f_h,\chi) + (f, v-\chi) + a_h(u_h,\chi) - a(u_h,\chi) - a(u_h, v-\chi) \end{aligned} \tag{5.2}$$

for all $\chi \in V_h$. Moreover, we observe that integration by parts yields

$$a(u_h,w) = -(\nabla\cdot\nabla(\Pi^\nabla u_h), w) + \sum_{E\in\mathcal{S}_h}\int_E [\![\nabla(\Pi^{\nabla,K}u_h)]\!] w ds + (\nabla(I-\Pi^{\nabla,K})u_h, \nabla w) \tag{5.3}$$

for all $w \in H^1_0(\Omega)$, where $\Pi^\nabla(\cdot)|_K = \Pi^{\nabla,K}(\cdot)$ for every $K \in \mathscr{K}_h$. Employing (5.2)-(5.3) we get

$$\begin{aligned} a(e,v) &= \sum_{K\in\mathcal{T}_h}((R_k, v-\chi)_K + (\theta_K, v-\chi)_K + B_K(u_h, v-\chi)) - \sum_{E\in\mathcal{S}_h}(J_E, v-\chi)_E \\ &\quad + (f-f_h,\chi) + a_h(u_h,\chi) - a(u_h,\chi) \end{aligned} \tag{5.4}$$

where

$$\begin{aligned} R_K &= (f_h + \nabla\cdot\nabla(\Pi^{\nabla,K}u_h)_K = f_h|_K, \\ \theta_K &= (f-f_h)_K, \\ B_K(w_h,v) &= (\nabla(I-\Pi^{\nabla,K})w_h, \nabla v)_K, \\ J_E &= [\![\nabla(\Pi^{\nabla,K}u_h)]\!]_E. \end{aligned}$$

Let $e_I = \mathfrak{I}_{C,0}e \in V_{h,0}$ be the quasi-interpolant of e satisfying the analogous version to the estimates (4.15)-(4.16). Then we have

$$\begin{aligned} \|\nabla e\|^2_{L^2(\Omega)} &= \sum_{K\in\mathcal{T}_h}\Big\{(R_K, e-e_I)_{L^2(K)} + (\theta_K, e-e_I)_{L^2(K)} + (f-f_h, e_I)_{L^2(K)} \\ &\quad + B_K(u_h, e-e_I) + (a^K_h(u_h,e_I) - a^K(u_h,e_I))\Big\} - \sum_{E\in\mathcal{S}_h}(J_E, e-e_I)_{L^2(E)} \\ &=: \sum_{K\in\mathcal{T}_h}(\mathtt{I}+\mathtt{II}+\mathtt{III}+\mathtt{IV}+\mathtt{V}) - \sum_{E\in\mathcal{S}_h}\mathtt{VI}. \end{aligned} \tag{5.5}$$

Let us now estimate the above terms. Employing Cauchy-Schwarz inequality together with the analogous estimate to (4.15) we have

$$\mathtt{I} \lesssim \|R_K\|_{L^2(K)}\alpha_K^{-1}\left(\lambda_{K,1}\,\mathbf{r}^\top_{K,1}\,G_K(e)\,\mathbf{r}_{K,1} + \lambda_{K,2}\,\mathbf{r}^\top_{K,2}\,G_K(e)\,\mathbf{r}_{K,2}\right)^{1/2}. \tag{5.6}$$

Similarly, employing the analogous estimate to (4.16), we have

$$\mathtt{VI} \lesssim \|J_E\|_{L^2(E)}\alpha_K^{-1}\left(\frac{|E|}{|K|}\right)^{1/2}\left(\lambda_{K,1}\,\mathbf{r}^\top_{K,1}\,G_K(e)\,\mathbf{r}_{K,1} + \lambda_{K,2}\,\mathbf{r}^\top_{K,2}\,G_K(e)\,\mathbf{r}_{K,2}\right)^{1/2}. \tag{5.7}$$

Combining `II` and `III` yields

$$\begin{aligned} \mathtt{II}+\mathtt{III} &= (f-f_h, e)_K = (f-f_h, e-\Pi^{0,K}_0 e)_K \\ &\leqslant \|f-f_h\|_{L^2(K)}\|e-\Pi^{0,K}_0 e\|_{L^2(K)} \\ &\lesssim \|f-f_h\|_{L^2(K)}\|\alpha_K^{-1}\Lambda_K^{1/2}U_K^\top\nabla e\|_{L^2(K)} \\ &= \|f-f_h\|_{L^2(K)}\alpha_K^{-1}\left(\lambda_{K,1}\,\mathbf{r}^\top_{K,1}\,G_K(e)\,\mathbf{r}_{K,1} + \lambda_{K,2}\,\mathbf{r}^\top_{K,2}\,G_K(e)\,\mathbf{r}_{K,2}\right)^{1/2} \end{aligned}$$

according to Lemma 3.5. We now focus on the term `IV`. Remembering (5.1) we have

$$\begin{aligned} \mathtt{IV} &\leqslant \|\nabla(I-\Pi^{\nabla,K})u_h\|_{L^2(K)}\|\nabla(e-e_I)\|_{L^2(K)} \\ &\leqslant \left(\frac{\lambda_{K,1}}{\lambda_{K,2}}\right)^{\frac{1}{4}}\left(S^K((I-\Pi^{\nabla,K})u_h, (I-\Pi^{\nabla,K})u_h)\right)^{\frac{1}{2}}\|\nabla(e-e_I)\|_{L^2(K)} \\ &\lesssim \left(\frac{\lambda_{K,1}}{\lambda_{K,2}}\right)^{\frac{3}{4}}\left(S^K((I-\Pi^{\nabla,K})u_h, (I-\Pi^{\nabla,K})u_h)\right)^{\frac{1}{2}}\|\nabla e\|_{L^2(\omega_K)} \end{aligned} \tag{5.8}$$

where in the last step we employed the analogous version to (4.13) for $\mathfrak{I}_{C,0}$. Finally, we consider the term $\mathtt{V}$. It is immediate to verify that it holds

$$\mathtt{V} = \underbrace{(\nabla(I-\Pi^{\nabla,K})u_h, \nabla e_I)_K}_{\mathtt{V}_1} - \underbrace{S^K((I-\Pi^{\nabla,K})u_h, (I-\Pi^{\nabla,K})e_I)}_{\mathtt{V}_2}. \tag{5.9}$$

Employing the Cauchy-Schwarz inequality together with (5.1) and the analogous estimate to (4.13) we have

$$\begin{aligned}
|\mathtt{V}_1| &\leqslant \|\nabla(I-\Pi^{\nabla,K})u_h\|_{L^2(K)}\|\nabla e_I\|_{L^2(K)} \\
&\leqslant \left(\frac{\lambda_{K,1}}{\lambda_{K,2}}\right)^{\frac{1}{4}} \left(S^K((I-\Pi^{\nabla,K})u_h, (I-\Pi^{\nabla,K})u_h)\right)^{\frac{1}{2}} \|\nabla e_I\|_{L^2(K)} \\
&\lesssim \left(\frac{\lambda_{K,1}}{\lambda_{K,2}}\right)^{\frac{3}{4}} \left(S^K((I-\Pi^{\nabla,K})u_h, (I-\Pi^{\nabla,K})u_h)\right)^{\frac{1}{2}} \|\nabla e\|_{L^2(\omega_K)}.
\end{aligned}$$

Employing (5.1) and (4.13) we have

$$\begin{aligned}
|\mathtt{V}_2| &\leqslant \left(\frac{\lambda_{K,1}}{\lambda_{K,2}}\right)^{\frac{1}{4}} S^K((I-\Pi^{\nabla,K})u_h, (I-\Pi^{\nabla,K})u_h)^{\frac{1}{2}} \|\nabla(I-\Pi^{\nabla,K})e_I\|_{L^2(K)} \\
&\leqslant \left(\frac{\lambda_{K,1}}{\lambda_{K,2}}\right)^{\frac{1}{4}} S^K((I-\Pi^{\nabla,K})u_h, (I-\Pi^{\nabla,K})u_h)^{\frac{1}{2}} \|\nabla e_I\|_{L^2(K)} \\
&\lesssim \left(\frac{\lambda_{K,1}}{\lambda_{K,2}}\right)^{\frac{3}{4}} S^K((I-\Pi^{\nabla,K})u_h, (I-\Pi^{\nabla,K})u_h)^{\frac{1}{2}} \|\nabla e\|_{L^2(\omega_K)}.
\end{aligned}$$

Hence,

$$\mathtt{V} \lesssim \left(\frac{\lambda_{K,1}}{\lambda_{K,2}}\right)^{\frac{3}{4}} S^K((I-\Pi^{\nabla,K})u_h, (I-\Pi^{\nabla,K})u_h)^{\frac{1}{2}} \|\nabla e\|_{L^2(\omega_K)}.$$

Using that the cardinality of ω_K is uniformly bounded (i.e. the number of edges of each polygon is uniformly bounded) yield the thesis. □

In the following, we focus on the computation of $G_K(e)$. In order to deal with this term we employ Zienkiewicz-Zhu (ZZ) error estimator (see, e.g., Zhu & Zienkiewicz (1990); Zienkiewicz & Zhu (1992a,b)) which yields

$$G_K(e) \simeq \tilde{G}_K(u_h) := \sum_{K'\subset\omega_K} \begin{pmatrix} \int_{K'} (\eta_1^{ZZ}(u_h))^2\, d\mathbf{x} & \int_{K'} \eta_1^{ZZ}(u_h)\eta_2^{ZZ}(u_h)\, d\mathbf{x} \\ \int_{K'} \eta_1^{ZZ}(u_h)\eta_2^{ZZ}(u_h)\, d\mathbf{x} & \int_{K'} (\eta_2^{ZZ}(u_h))^2\, d\mathbf{x} \end{pmatrix}, \tag{5.10}$$

with $\eta_i^{ZZ}(u_h)$ to be properly defined. Here, setting $\Pi^{\nabla,h}|_K = \Pi^{\nabla,K}$, we take

$$\eta_i^{ZZ}(u_h) = (I-\Pi_h^{ZZ})(\partial_{x_i}(\Pi^{\nabla,h}u_h)),$$

$i=1,2$ where for every vertex v of K' we set

$$\Pi_h^{ZZ}(\partial_{x_i}(\Pi^{\nabla,h}u_h))(\mathsf{v}) = \frac{1}{\sum_{K'':\mathsf{v}\in K''}|K''|} \sum_{K'':\mathsf{v}\in K''} |K''|\partial_{x_i}(\Pi^{\nabla,K''}u_h)_{|K''}.$$

We employ the above vertex values $\Pi_h^{ZZ}(\partial_{x_i}(\Pi^{\nabla,h}u_h))(\mathsf{v})$ to construct, via e.g. least square fitting, a linear polynomial on K' that we denote by $\Pi_h^{ZZ}(\partial_{x_i}(\Pi^{\nabla,h}u_h))_{|K'}$. This latter enters in the construction of $\eta_i^{ZZ}(u_h)$ and thus it is employed to approximate $G_K(e)$.

In the sequel we briefly comment on the viability of the approximation in (5.10). In particular, we restrict ourself to regular isotropic meshes (see Section 6 for a numerical investigation of the anisotropic case) and we prove the following estimate in the spirit of the results obtained in Guo *et al.* (2019); Chi *et al.* (2019).

PROPOSITION 5.2 Let $u_h \in V_h$ be the VEM approximation on regular isotropic meshes to the solution u of (2.1) and let $e = u - u_h$. Then, for any $K \in \mathscr{T}_h$, if $u \in H^2(\Omega)$,

$$\left\| \begin{pmatrix} \eta_1^{ZZ}(u_h) \\ \eta_2^{ZZ}(u_h) \end{pmatrix} - \nabla e \right\|_{L^2(\omega_K)} \lesssim h_{\omega_K} |u|_{H^2(\omega_K)} + \left(\sum_{i=1}^{n_{\omega_K}} \left(u(\mathsf{v}_{i,\omega_K}) - u_h(\mathsf{v}_{i,\omega_K}) \right)^2 \right)^{\frac{1}{2}}, \tag{5.11}$$

where $h_{\omega_K} = \max_{K' \in \omega_K} h_{K'}$, v_{i,ω_K} is the i-th vertex in $\overline{\omega}_K$ and n_{ω_K} is the number of such vertices.

Proof. For the sake of clarity, in the following we use the symbol Π_h^{ZZ} applied to a vector to denote the application of the operator Π_h^{ZZ} to each component of the vector. Moreover, let $u_I \in V_h$ be the VEM interpolant of the solution u (see Beirão da Veiga *et al.* (2016); Cangiani *et al.* (2017b)). By the triangle inequality, using the well established approximation properties of the VEM interpolant and of L^2 projectors, we get

$$\begin{aligned}
\left\| \begin{pmatrix} \eta_1^{ZZ}(u_h) \\ \eta_2^{ZZ}(u_h) \end{pmatrix} - \nabla e \right\|_{L^2(\omega_K)} &= \|\nabla \Pi^{\nabla,h} u_h - \Pi_h^{ZZ} \nabla \Pi^{\nabla,h} u_h - \nabla u + \nabla u_h\|_{L^2(\omega_K)} \\
&\leqslant \|\nabla \Pi^{\nabla,h} u_h - \nabla \Pi^{\nabla,h} u\|_{L^2(\omega_K)} + \|\nabla \Pi^{\nabla,h} u - \nabla u\|_{L^2(\omega_K)} \\
&\quad + \|\Pi_h^{ZZ} \nabla \Pi^{\nabla,h} u_h - \nabla u_h\|_{L^2(\omega_K)} \\
&\lesssim \|\nabla u_h - \nabla u\|_{L^2(\omega_K)} + \|\nabla \Pi^{\nabla,h} u - \nabla u\|_{L^2(\omega_K)} + \|\Pi_h^{ZZ} \nabla \Pi^{\nabla,h} u_h - \nabla u_h\|_{L^2(\omega_K)} \\
&\lesssim \|\nabla u_h - \nabla u_I\|_{L^2(\omega_K)} + \|\nabla u - \nabla u_I\|_{L^2(\omega_K)} + \|\nabla \Pi^{\nabla,h} u - \nabla u\|_{L^2(\omega_K)} \\
&\quad + \|\Pi_h^{ZZ} \nabla \Pi^{\nabla,h} u_h - \nabla u_h\|_{L^2(\omega_K)} \\
&\lesssim h_{\omega_K} |u|_{H^2(\omega_K)} + \|\nabla u_h - \nabla u_I\|_{L^2(\omega_K)} + \|\Pi_h^{ZZ} \nabla \Pi^{\nabla,h} u_h - \nabla u_h\|_{L^2(\omega_K)},
\end{aligned} \tag{5.12}$$

where we used the regularity of the mesh, which implies that the number of elements in ω_K is uniformly bounded. The last norm can be estimated introducing the $L^2(\omega_K)$ projection on polynomials of degree 2, denoted by $\Pi_2^{0,\omega_K} : L^2(\omega_K) \to \mathbb{P}^2(\omega_K)$, and using the continuity of the Π_h^{ZZ} operator and its consistency on continuous polynomials of degree 1, which implies

$$\Pi_h^{ZZ} \nabla \Pi_2^{0,\omega_K} u = \nabla \Pi_2^{0,\omega_K} u .$$

We get

$$\begin{aligned}
\|\Pi_h^{ZZ} \nabla \Pi^{\nabla,h} u_h - \nabla u_h\|_{L^2(\omega_K)} &\leqslant \|\Pi_h^{ZZ} \nabla \Pi^{\nabla,h} u_h - \Pi_h^{ZZ} \nabla \Pi_2^{0,\omega_K} u\|_{L^2(\omega_K)} + \|\nabla \Pi_2^{0,\omega_K} u - \nabla u\|_{L^2(\omega_K)} \\
&\quad + \|\nabla u - \nabla u_I\|_{L^2(\omega_K)} + \|\nabla u_I - \nabla u_h\|_{L^2(\omega_K)} \\
&\lesssim \|\nabla \Pi^{\nabla,h} u_h - \nabla \Pi_2^{0,\omega_K} u\|_{L^2(\omega_K)} + h_{\omega_K} |u|_{H^2(\omega_K)} + \|\nabla u_I - \nabla u_h\|_{L^2(\omega_K)} \\
&\lesssim \|\nabla \Pi^{\nabla,h} u_h - \nabla \Pi^{\nabla,h} u\|_{L^2(\omega_K)} + \|\nabla \Pi^{\nabla,h} u - \nabla \Pi_2^{0,\omega_K} u\|_{L^2(\omega_K)} \\
&\quad + h_{\omega_K} |u|_{H^2(\omega_K)} + \|\nabla u_I - \nabla u_h\|_{L^2(\omega_K)} \\
&\lesssim \|\nabla u_h - \nabla u\|_{L^2(\omega_K)} + \|\nabla \Pi^{\nabla,h} u - \nabla u\|_{L^2(\omega_K)} + \|\nabla u - \nabla \Pi_2^{0,\omega_K} u\|_{L^2(\omega_K)} \\
&\quad + h_{\omega_K} |u|_{H^2(\omega_K)} + \|\nabla u_I - \nabla u_h\|_{L^2(\omega_K)} \\
&\lesssim \|\nabla u_I - \nabla u\|_{L^2(\omega_K)} + h_{\omega_K} |u|_{H^2(\omega_K)} + \|\nabla u_h - \nabla u_I\|_{L^2(\omega_K)} \\
&\lesssim h_{\omega_K} |u|_{H^2(\omega_K)} + \|\nabla u_h - \nabla u_I\|_{L^2(\omega_K)},
\end{aligned} \tag{5.13}$$

where in the estimate of $\|\nabla u - \nabla \Pi_2^{0,\omega_K} u\|_{L^2(\omega_K)}$ we used the regularity of the mesh, which implies that the diameter of ω_K scales as h_{ω_K} and that the regularity of ω_K depends on the regularity of its elements. Finally, we are left to estimate the norm $\|\nabla u_h - \nabla u_I\|_{L^2(\omega_K)}$, which is present both in (5.12) and (5.13). By standard scaling arguments (see Chen & Huang (2018)), denoting by $\Xi_i^{\omega_K}$ the operator selecting the i-th degree of freedom in ω_K, with $i = 1, \ldots, n_{\omega_K}$, we get

$$\|\nabla u_h - \nabla u_I\|_{L^2(\omega_K)}^2 \lesssim \sum_{i=1}^{n_{\omega_K}} \left(\Xi_i^{\omega_K}(u_h) - \Xi_i^{\omega_K}(u_I) \right)^2 .$$

We conclude by observing that, since $u \in H^2(\omega_K)$ by hypothesis, then u is continuous and the nodal degrees of freedom of u_I coincide with the values of u at the vertices of ω_K. □

6. Numerical Results

In this section we assess the behavior of the error estimate on three test cases. We recall that, according to the previous section (cf. Proposition 5.1), the estimator is defined as:

$$\eta_h = \left(\sum_{K\in\mathscr{T}_h} \eta_K^2 + \sum_{E\in\mathscr{S}_h} \xi_E^2 + \sum_{K\in\mathscr{T}_h} \sigma_K^2 \right)^{1/2}, \tag{6.1}$$

where

$$\begin{aligned}
\eta_K^2 &= \|R_K\|_{L^2(K)} \alpha_K^{-1} \left(\lambda_{K,1}\, \mathbf{r}_{K,1}^\top G_K(e)\, \mathbf{r}_{K,1} + \lambda_{K,2}\, \mathbf{r}_{K,2}^\top G_K(e)\, \mathbf{r}_{K,2} \right)^{1/2}, \\
\xi_E^2 &= \|J_E\|_{L^2(E)} \max_{K:\, E\subset\partial K} \alpha_K^{-1} \left(\frac{|E|}{|K|} \right)^{1/2} \left(\lambda_{K,1}\, \mathbf{r}_{K,1}^\top G_K(e)\, \mathbf{r}_{K,1} + \lambda_{K,2}\, \mathbf{r}_{K,2}^\top G_K(e)\, \mathbf{r}_{K,2} \right)^{1/2},
\end{aligned}$$

and σ_K is given by

$$\tilde{\sigma}_K^2 = S^K((I-\Pi^{\nabla,K})u_h, (I-\Pi^{\nabla,K})u_h), \tag{6.2}$$

$$\sigma_K^2 = M_K^2 \tilde{\sigma}_K^2. \tag{6.3}$$

To highlight the advantage of using an anisotropic adaptive process, we compare our results with the ones obtained by refining the mesh with the following isotropic error estimate:

$$\eta_h^{\mathrm{iso}} = \left(\sum_{K\in\mathscr{T}_h} h_K^2 \|R_K\|_{L^2(K)}^2 + \sum_{E\in\mathscr{S}_h} h_E \|J_E\|_{L^2(E)}^2 + \sum_{K\in\mathscr{T}_h} \tilde{\sigma}_K^2 \right)^{\frac{1}{2}}, \tag{6.4}$$

see Berrone & Borio (2017); Cangiani *et al.* (2017b).
We also introduce the following *heuristically scaled estimator*

$$\eta_h^{\mathrm{heur}} = \left(\sum_{K\in\mathscr{T}_h} \eta_K^2 + \sum_{E\in\mathscr{S}_h} \xi_E^2 + \sum_{K\in\mathscr{T}_h} \tilde{\sigma}_K^2 \right)^{\frac{1}{2}}, \tag{6.5}$$

that differs from η_h for the presence of the unscaled stabilization terms $\tilde{\sigma}_K^2$.

In all the test cases, we consider (2.1) with $\Omega = (0,1)\times(0,1)$. All the three proposed tests have a boundary layer and are solved using VEM of order 1 and 2. We remark that the extension of the anisotropic a posteriori framework developed in the previous section to the case of VEM of order 2 (see Beirão da Veiga *et al.* (2013) for details on the definition of the approximation spaces) is straightforward. In the first two test cases the solution is purely anisotropic while in the last test there is both an isotropic structure and an anisotropic layer. Before presenting the results of the computations, we describe in detail the cell refinement strategy. To simplify the implementation of the anisotropic mesh refinement process, that in presence of very general elements may become computationally demanding, we restrict ourselves to convex elements. The efficient implementation of the mesh refinement process in the general case is under investigation.

6.1 *Cell refinement strategy*

The anisotropic adaptive VEM hinges upon the classical paradigm

$$\ldots \to \texttt{SOLVE} \to \texttt{ESTIMATE} \to \texttt{MARK} \to \texttt{REFINE} \to \ldots$$

The module `MARK` is based on the Dörfler strategy, see, e.g., Nochetto & Veeser (2012) for more details. All numerical tests have been run with marking parameter equal to $1/2$.

In the sequel we focus on the description of the module `REFINE`, see Algorithm 1 below. We aim at designing a refinement strategy that reduces the size of the element along the direction of the gradient of

the error (thus cutting in the orthogonal direction), while preventing an unnecessary increase of the aspect ratio of the polygon. The approach here applied extends the strategy presented in Berrone *et al.* (2019) (cf., e.g., Habashi *et al.* (2000) and Georgoulis *et al.* (2009) for refinement strategies in the case of triangular and quadrilateral elements, respectively).

More precisely, for each marked polygon K, we compute: (a) the eigenvalues $\lambda_{K,1}$ and $\lambda_{K,2}$ ($\lambda_{K,1} \geqslant \lambda_{K,2}$) of the covariance matrix $M_{\text{Cov}} = M_{\text{Cov}}(K)$ together with the corresponding eigenvectors $\mathbf{r}_{K,i}$, $i = 1,2$; (b) the eigenvalues $\lambda_{G,1}$ and $\lambda_{G,2}$ ($\lambda_{G,1} \geqslant \lambda_{G,2}$) of the matrix $G_K = G_K(e)$ together with the corresponding eigenvectors $\mathbf{r}_{G,i}$, $i = 1,2$. The matrix G_K is computed by resorting to the ZZ approximation, cf. (5.10) for VEM of order 1 (the case of VEM of order 2 simply requires the use of a quadratic least square fitting). We notice that large values of $\lambda_{G,1}/\lambda_{G,2}$ indicate a local anisotropic behaviour of the gradient of the error, whereas large values of $\lambda_{K,1}/\lambda_{K,2}$ are associated to anisotropic elements.

If $(\lambda_{G,1}/\lambda_{G,2}) \geqslant (\lambda_{K,1}/\lambda_{K,2})$, then the refinement strategy cuts the polygon K along $\mathbf{r}_{G,2}$, otherwise it cuts along $\mathbf{r}_{K,2}$.

Whenever $\lambda_{G,1}/\lambda_{G,2} \geqslant \lambda_{K,1}/\lambda_{K,2}$ the refinement strategy takes advantage of the pronounced anisotropic behaviour of the gradient of the error, whereas if $\lambda_{K,1}/\lambda_{K,2}$ dominates then the aspect ratio of the element is reduced. Heuristically speaking, when $\lambda_{K,1}/\lambda_{K,2}$ dominates on $\lambda_{G,1}/\lambda_{G,2}$ the module `REFINE` aims at identifying a situation where the anisotropy of the element is too pronounced (and possibly unnecessary) with respect to the (anisotropic) behaviour of the gradient of the error. A typical situation could be the presence of an anisotropic element in a region where an isotropic refinement is needed (i.e. the gradient of the error does not exhibit any preferential direction).

Finally, we remark that whenever the estimator η_h^{iso} is used to drive the adaptive procedure, the marked polygon is always cut along the direction $\mathbf{r}_{K,2}$.

Algorithm 1 The Module `REFINE`

Given a marked cell K

1: Compute the barycenter $\bar{\mathbf{x}}_K$
2: Compute the tensor G_K
3: Compute the covariance matrix M_{Cov}
4: Compute the eigenvalues of the two tensors
5: **if** $(\lambda_{G,1}/\lambda_{G,2}) \geqslant (\lambda_{K,1}/\lambda_{K,2})$ **then**
6: Build a straight line passing through $\bar{\mathbf{x}}_K$ and parallel to $\mathbf{r}_{G,2}$
7: **else**
8: Build a straight line passing through $\bar{\mathbf{x}}_K$ and parallel to $\mathbf{r}_{K,2}$
9: **end if**
10: Refine the cell

In the following test cases we employ

$$\tilde{e} = \|\nabla(u - \Pi_k^0 u_h)\|_\Omega \qquad k = 1,2$$

as a measure of the exact error and we iterate the adaptive process until $\tilde{e} \leqslant 10^{-3}$.

6.2 *Test case 1*

In the first test we set the forcing term in such a way that the exact solution is given by

$$u(x,y) = 10^{-6} x(1-x)(1-y)(\mathrm{e}^{10x} - 1)(\mathrm{e}^{10y} - 1)\,.$$

In Figure 1 we plot the exact solution, that displays a peak in the top-right corner of the domain, with boundary layers in the x and y directions. In Figure 2 we report the behavior of the error estimator η_h defined as in (6.1) when the adaptive process is run using η_h as estimator, based on employing both VEM of order 1 (cf. Figure 2a) and of order 2 (cf. Figure 2b). We notice that the estimator η_h exhibits the correct rates of convergence, but displays some mild oscillations. The origin of the oscillations is further investigated in Figure 3 where we display the three components of the estimator: we observe that the oscillations are due to the term σ_K, in view of of its dependence on the aspect ratio of the elements through

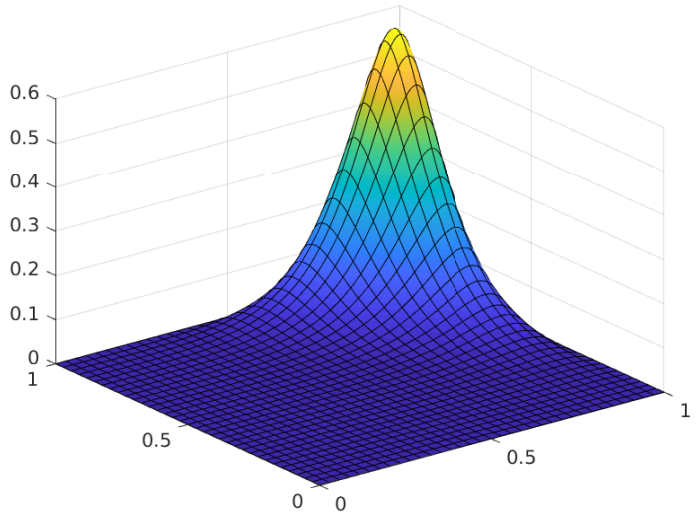

FIG. 1: Test case 1. Plot of the exact solution

the term M_K. In this respect, as we can see from Figure 4, the estimator η_h^{heur} (where we set $M_k = 1$, cf. (6.5)) does not present such oscillations and preserves the correct rate of convergence. Finally, in Figures 2 and 4 we also display the behaviour of the isotropic estimator η_h^{iso}, that, as expected, requires a larger number of degrees of freedom to reach the desired tolerance, compared to both choices of the anisotropic estimator.

In Figure 5 we report the color-plot of the solutions and the meshes at the beginning of the adaptive process, whereas in Figure 6 we show the solutions and the meshes obtained at intermediate adaptive steps by both estimators η_h and η_h^{heur} for VEM or order 1 and 2. We can see that the meshes induced by the two estimators are quite similar. A zoom of a detail of the computed anisotropic mesh as well as the computed solution at the final adaptive step, are reported in Figures 7 and 8, for the estimators η_h and η_h^{heur} respectively, again employing VEM of order 1 and 2. The obtained meshes are quite similar, but the adaptive algorithm driven by the estimator η_h required more refinement steps to satisfy the stopping criterium.

Finally, we explore the approximation of $G_K(e)$ in (5.10) (see also Proposition 5.2). From the results reported in Figure 9 and noticing that $\max_{K\in\mathcal{T}_h} \|G_K(e)\|_\infty$ scales as $\|\nabla e\|^2_{L^2(\Omega)}$, it is reasonable to infer the reliability of our approximation.

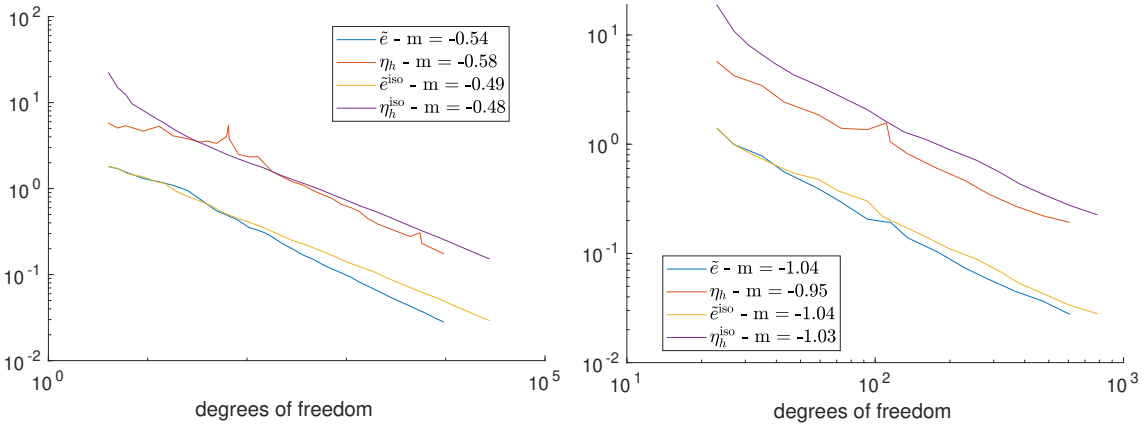

(a) VEM of order 1. (b) VEM of order 2

FIG. 2: Test case 1. Computed values of the estimator η_h, computed errors $\tilde{e}$ based on employing the exact solution, and corresponding computed convergence rates m as a function of the number of degrees of freedom. The results are compared with the analogous quantities obtained based on employing the isotropic error estimator η_h^{iso} defined in (6.4).

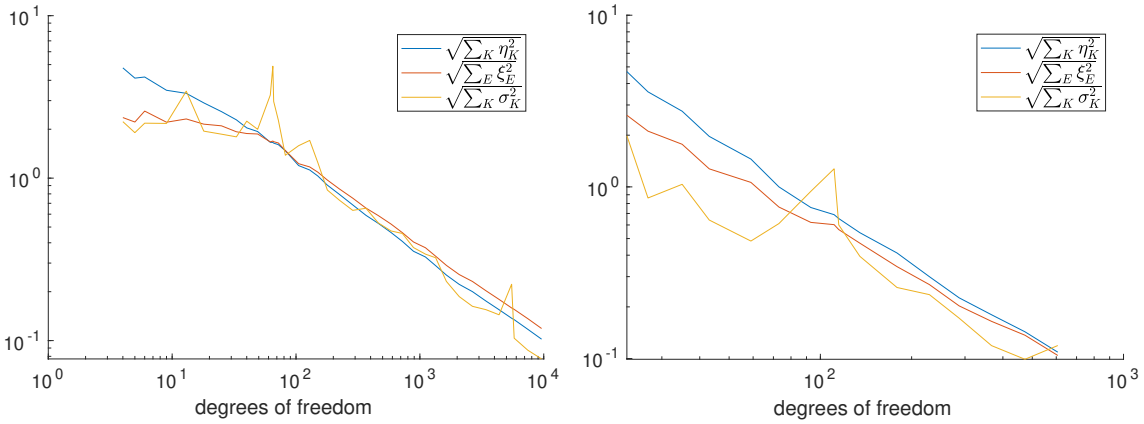

(a) VEM of order 1. (b) VEM of order 2.

FIG. 3: Test case 1. Components of the error estimator η_h as a function of the number of degrees of freedom, when the adaptive process is driven by the estimator η_h.

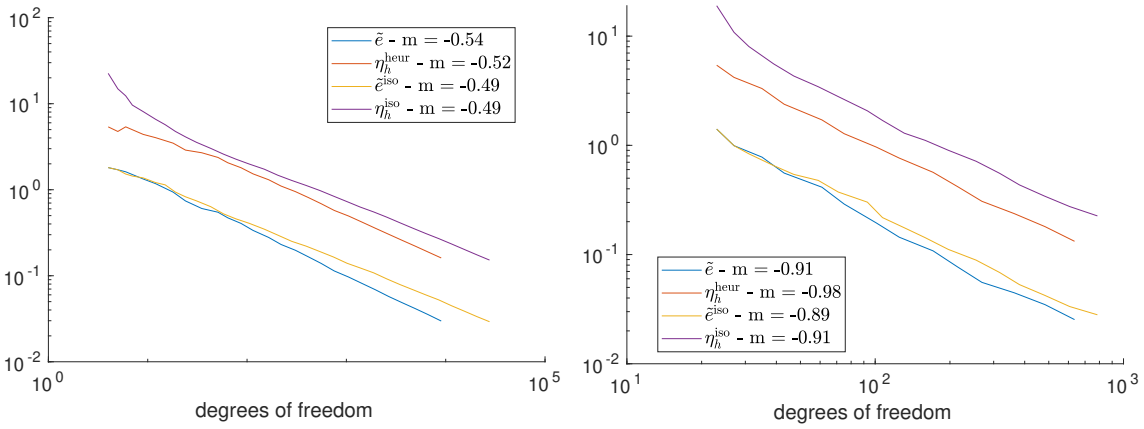

(a) VEM of order 1. (b) VEM of order 2

FIG. 4: Test case 1. Computed values of the estimator η_h^{heur}, computed errors $\widetilde{e}$ based on employing the exact solution, and corresponding computed convergence rates $\mathtt{m}$ (obtained through least square fitting) as a function of the number of degrees of freedom. The results are compared with the analogous quantities obtained based on employing the isotropic error estimator η_h^{iso} defined in (6.4).

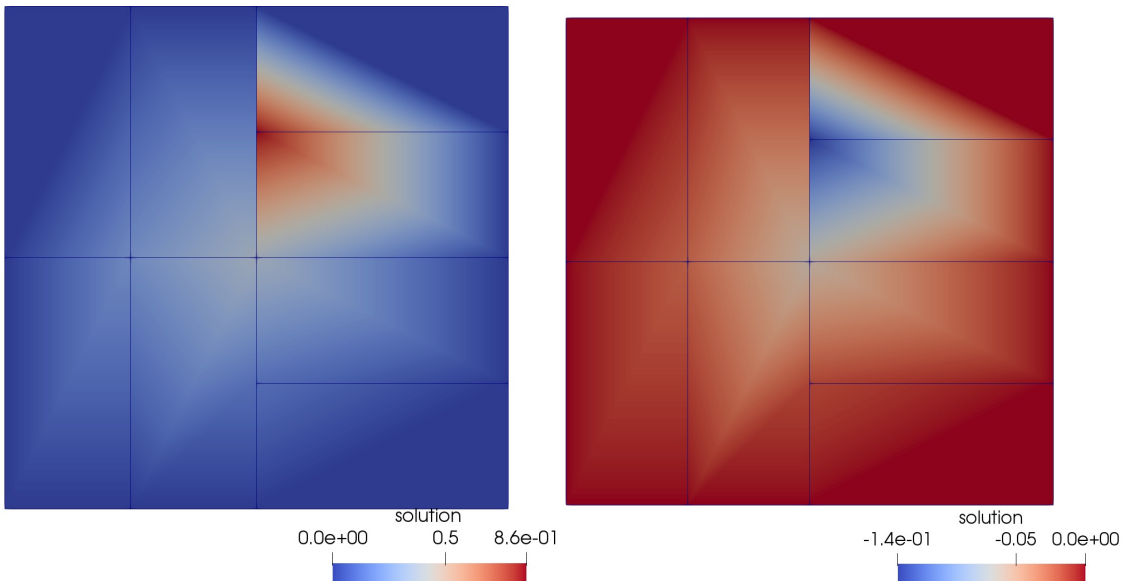

(a) VEM of order 1. (b) VEM order 2.

FIG. 5: Test case 1. Initial meshes.

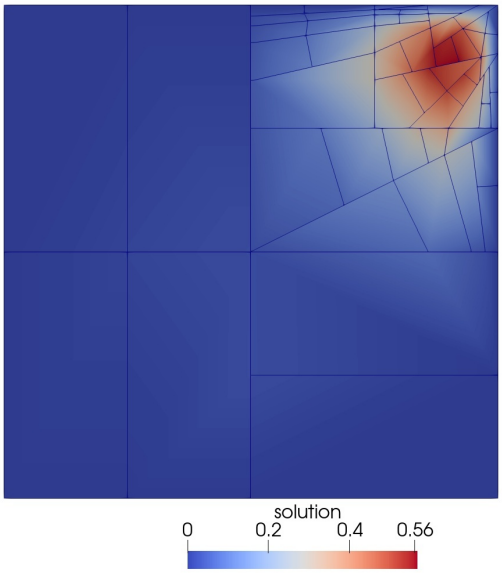

(a) VEM of order 1. Estimator η_h. Adaptive step n. 12.

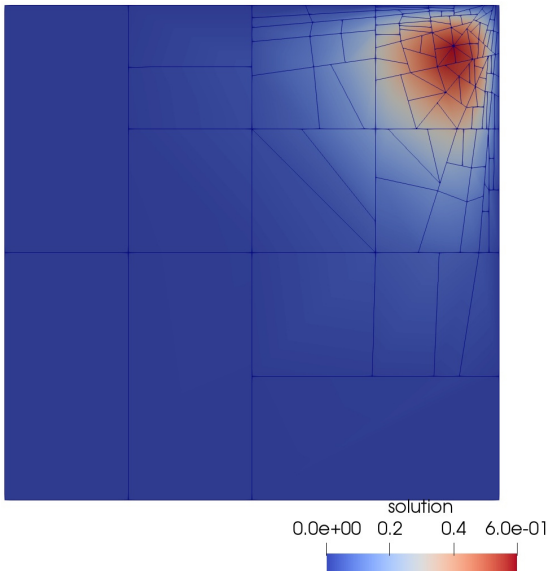

(b) VEM of order 1. Estimator η_h^{heur}. Adaptive step n. 12.

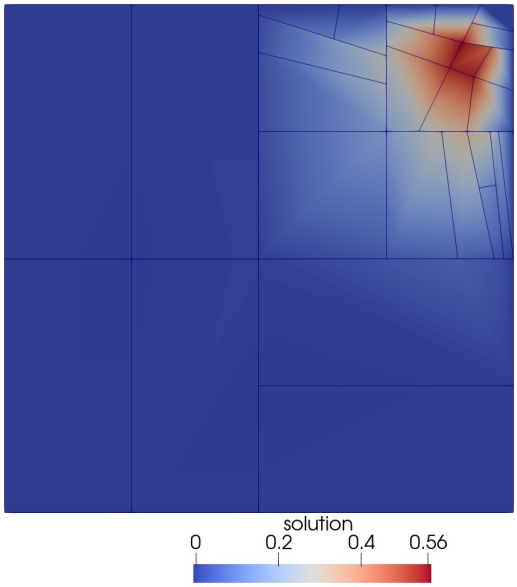

(c) VEM order 2. Estimator η_h. Adaptive step n. 7.

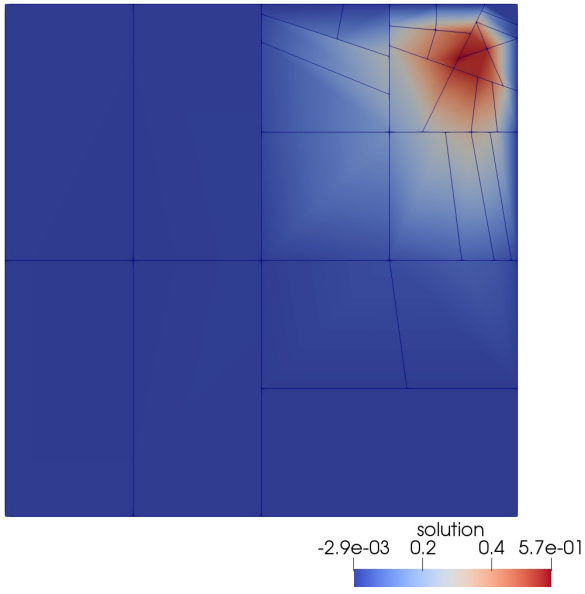

(d) VEM order 2. Estimator η_h^{heur}. Adaptive step n. 7.

FIG. 6: Test case 1. Computed solutions and corresponding anisotropic grids at different steps of the adaptive algorithm based on employing the estimators defined in (6.1) and (6.5) to drive the adaptive algorithm.

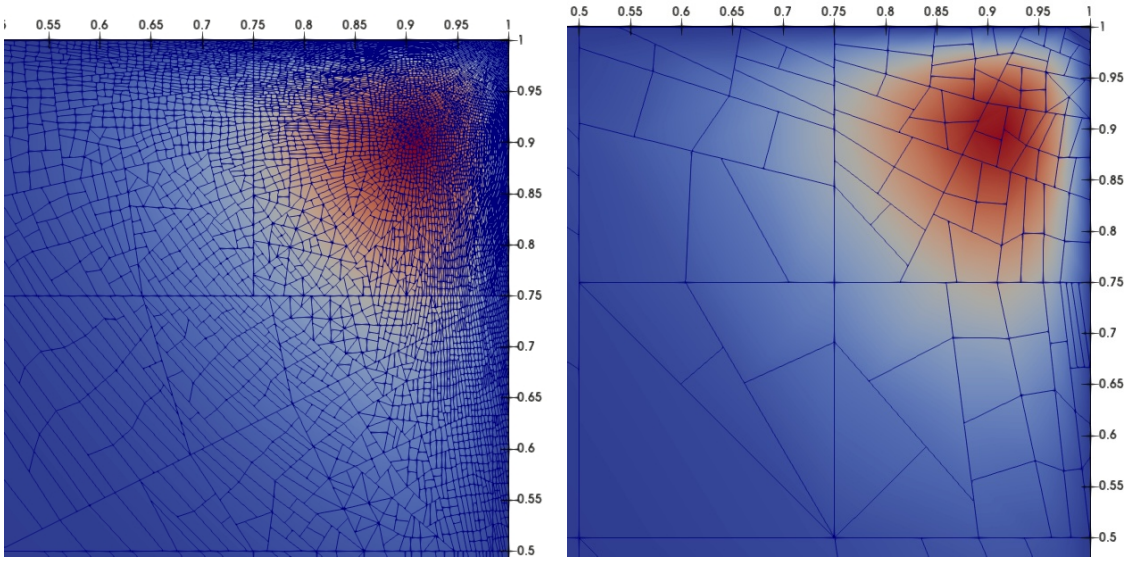

(a) VEM order 1. Adaptive step n. 36. (b) VEM order 2. Adaptive step n. 15

FIG. 7: Test case 1. Zoom of the computed solutions and corresponding anisotropic grids at the final step of the adaptive algorithm based on employing the estimator η_h defined in (6.1) to drive the adaptive algorithm.

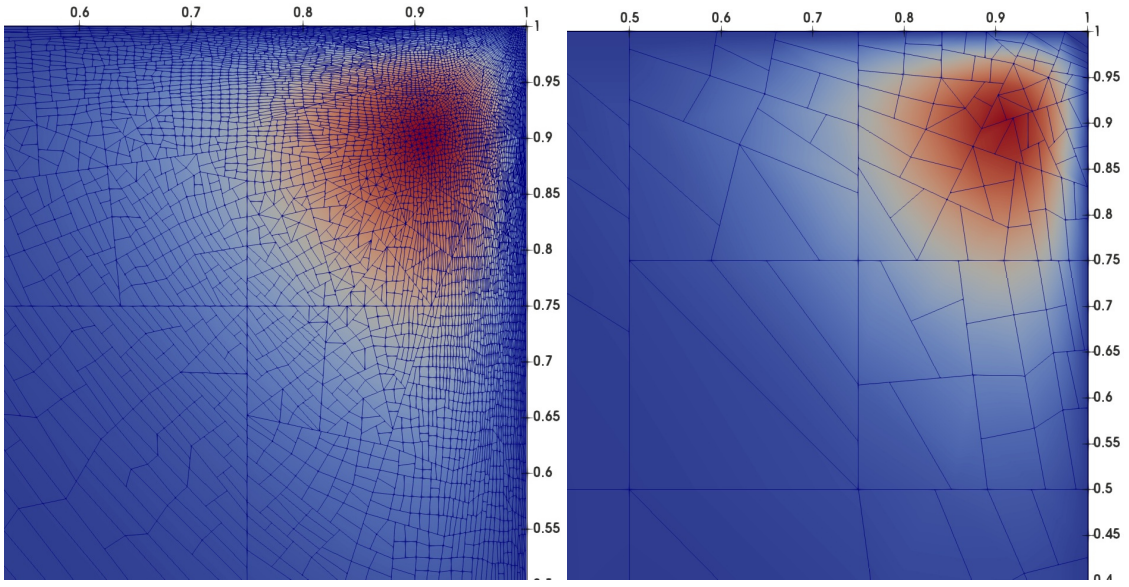

(a) VEM order 1. Adaptive step n. 25. (b) VEM order 2. Adaptive step n. 13

FIG. 8: Test case 1. Zoom of the computed solutions and corresponding anisotropic grids at the final step of the adaptive algorithm based on employing the *heuristically scaled estimator* η_h^{heur} defined in (6.5) to drive the adaptive algorithm.

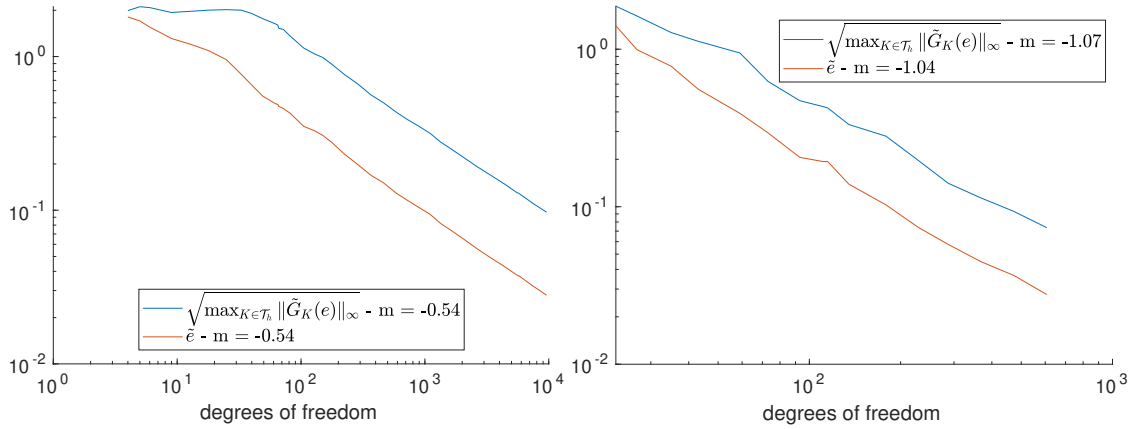

(a) VEM of order 1 (b) VEM of order 2

FIG. 9: Test case 1. Computed values of $\sqrt{\max_{K\in\mathcal{T}_h}\|\tilde{G}_K(u_h)\|_\infty}$ and computed values of $\tilde{e}$ when the adaptive process is driven by the estimator η_h, and corresponding computed convergence rates m as a function of the number of degrees of freedom.

6.3 *Test case 2*

We have repeated the same set of experiments of the previous section, now choosing the forcing term in such a way that the exact solution is given by

$$u(x,y) = 10^{-2}xy(1-x)(1-y)(\mathrm{e}^{10x}-1).$$

We notice that the exact solution of the proposed test case exhibits a steep boundary layer in the x-direction close to the right boundary of the domain (see Figure 10). Next, we report the color-plot of the computed

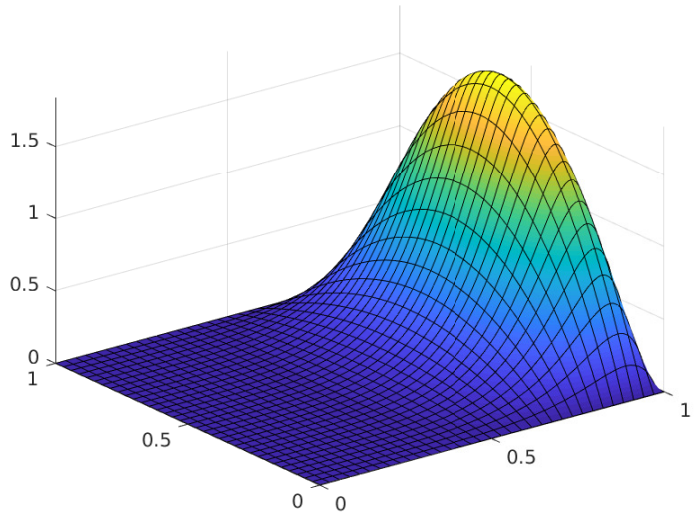

FIG. 10: Test case 2. Plot of the exact solution

solutions and the corresponding meshes at the initial step of the adaptive algorithm, and after 16 (resp. 9), iterations based on employing VEM of order 1 (resp. 2), and using the *heuristically scaled estimator* η_h^{heur} defined in (6.5) to drive the adaptive process; cf. Figure 11. A zoom of a detail of the computed anisotropic mesh as well as the corresponding computed solution at the final step of the adaptive algorithm are reported in Figure 12, again employing VEM of order 1 (Figure 12, top) and VEM of order 2 (Figure 12, bottom). Similar meshes are obtained using η_h; for brevity they are not reported here. Finally, we compare

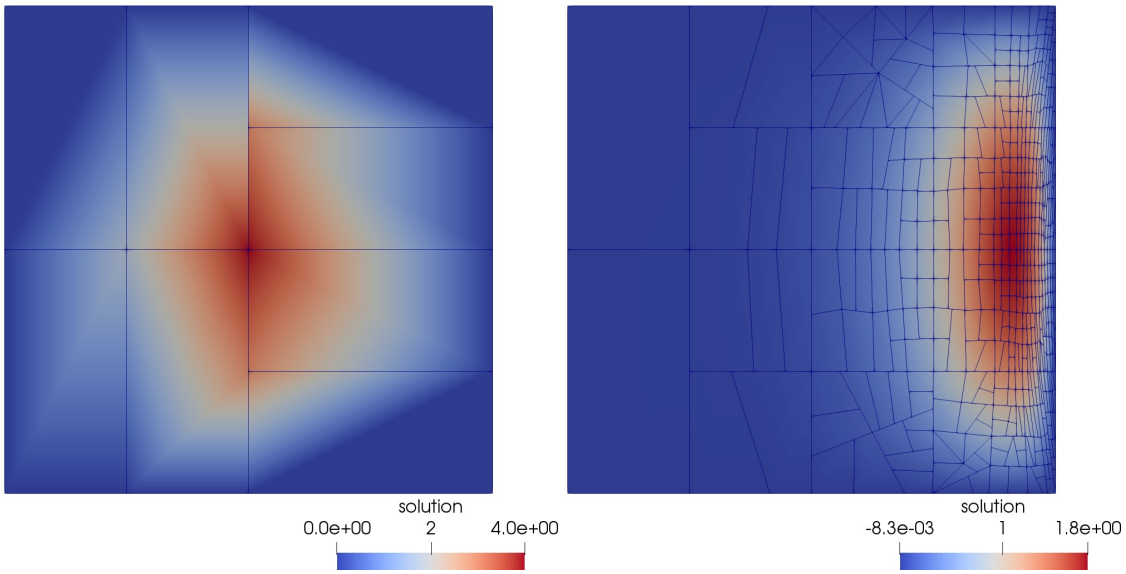

(a) VEM of order 1. Adaptive step n. 1.

(b) VEM of order 1. Adaptive step n. 16.

(c) VEM order 2. Adaptive step n. 1.

(d) VEM order 2. Adaptive step n. 9.

FIG. 11: Test case 2. Computed solutions and corresponding anisotropic grids at different steps of the adaptive algorithm based on employing the *heuristically scaled estimator* η_h^{heur} defined in (6.5) to drive the adaptive algorithm.

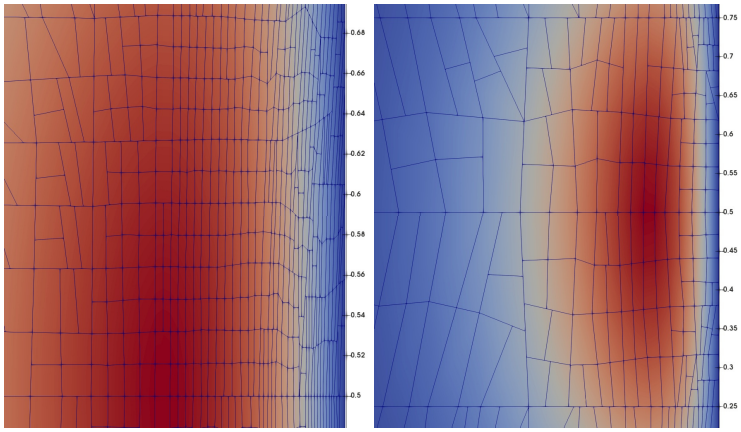

(a) VEM order 1. Adaptive step n. 21.

(b) VEM order 2. Adaptive step n. 13

FIG. 12: Test case 2. Zoom of the computed solutions and corresponding anisotropic grids at the final step of the adaptive algorithm based on employing the *heuristically scaled estimator* η_h^{heur} defined in (6.5) to drive the adaptive algorithm.

the behavior of the computed estimator and of the error as a function of the number of the degrees of freedom. In Figure 13 we show the estimator η_h and the corresponding error $\tilde{e}$ as functions of the number of degrees of freedom. As for the previous test, the estimator exhibits the correct rate of convergence but it displays some mild oscillations, that are not present when considering the *heuristically scaled estimator*; see Figure 14 where we report the estimator η_h^{heur} and the error $\tilde{e}$, plotted against the number of degrees of freedom as well as the computed convergence rates. As before, we compare these results with the analogous quantities obtained with the isotropic error estimator η_h^{iso} defined in (6.4). These results have been obtained with VEM of order 1, cf. Figures 13a and 14a and with VEM of order 2, cf. Figures 13b and 14b. We observe, as expected, that the isotropic adaptive process requires a larger number of degrees of freedom to reduce the error below a given tolerance compared with the anisotropic error estimator.

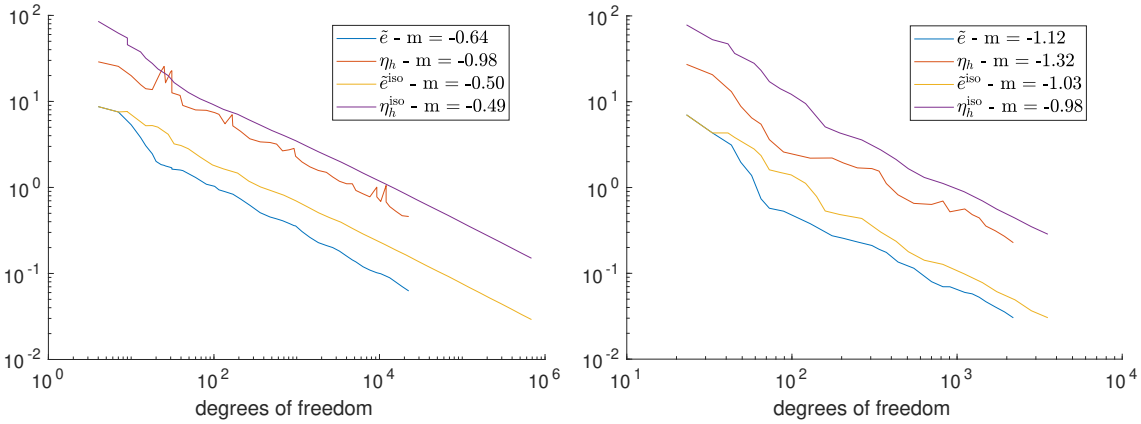

(a) VEM of order 1. (b) VEM of order 2

FIG. 13: Test case 2. Computed values of the estimator η_h, computed errors $\widetilde{e}$ based on employing the exact solution, and corresponding computed convergence rates m as a function of the number of degrees of freedom. The results are compared with the analogous quantities obtained based on employing the isotropic error estimator η_h^{iso} defined in (6.4).

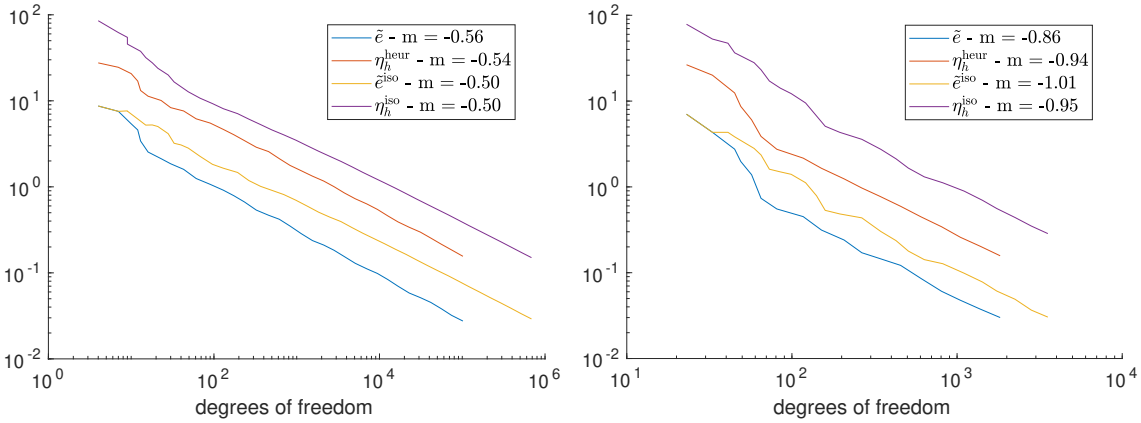

(a) VEM of order 1. (b) VEM of order 2

FIG. 14: Test case 2. Computed values of the estimator η_h^{heur}, computed errors $\widetilde{e}$ based on employing the exact solution, and corresponding computed convergence rates m as a function of the number of degrees of freedom. The results are compared with the analogous quantities obtained based on employing the isotropic error estimator η_h^{iso} defined in (6.4).

6.4 *Test case 3*

We have repeated the same set of experiments of the previous section, now choosing the forcing term in such a way that the exact solution is given by

$$u(x,y) = 10^{-2}xy(x-1)(y-1)(e^{10x} - 5000x + 4499),$$

that is obtained summing an isotropic bubble of the form

$$b(x,y) = 50x(1-y)y(0.9-x)(1-x)$$

to the solution of the second test case, cf. Figure 15. The manufactured exact solution exhibits a steep boundary layer in the x-direction close to the right side of the domain, which requires *anisotropic* mesh refinement to be efficiently treated and a bubble function in the left part of the domain, which asks for *isotropic* mesh refinement. Next, we report the color-plot of the computed solutions and the meshes obtained

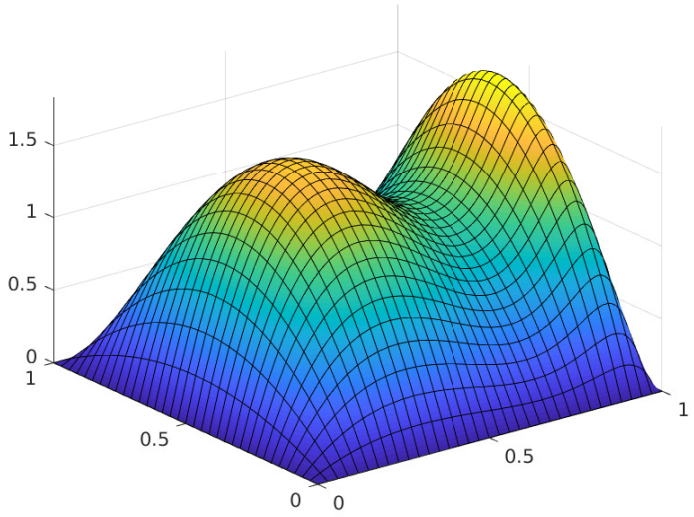

FIG. 15: Test case 3. Plot of the exact solution

at the initial step of the refinement process, and after 17 (resp. 9), iterations based on employing VEM of order 1 (resp. 2), and using the *heuristically scaled estimator* η_h^{heur} defined in (6.5) to drive the adaptive algorithm; Figure 16 (top) shows the results obtained with VEM of order 1, whereas in Figure 16 (bottom) we show the analogous computations obtained with VEM of order 2. A zoom of a detail of the computed solutions together with the corresponding computed anisotropic meshes at the final step of the adaptive algorithm are reported in Figure 17, again employing VEM of order 1 (left) and VEM of order 2 (right). Similar meshes are obtained using η_h; for brevity they are not reported here. The reported results show that the combination of isotropic and anisotropic mesh refinement is correctly captured by the adaptive algorithm. Finally, we compare the behavior of the computed estimator and of the error as a function of the number of the degrees of freedom. In Figure 18 we show the estimator η_h and the error $\tilde{e}$ as functions of the number of degrees of freedom. Again, the estimator features η_h some mild oscillations that are not present when the estimator estimator η_h^{heur} is employed; see Figure 19 where we report the estimator η_h^{heur} and the error $\tilde{e}$ versus the number of degrees of freedom, together with the computed convergence rates. These results have been obtained with VEM of order 1, cf. Figures 18a and 19a and with VEM of order 2, cf. Figures 18b and 19b. As before, we compare these results with the analogous ones obtained with the isotropic error estimator η_h^{iso} defined in (6.4). Again, as expected, the adaptive algorithm based on employing the anisotropic estimator guarantees a lower error compared with the isotropic one.

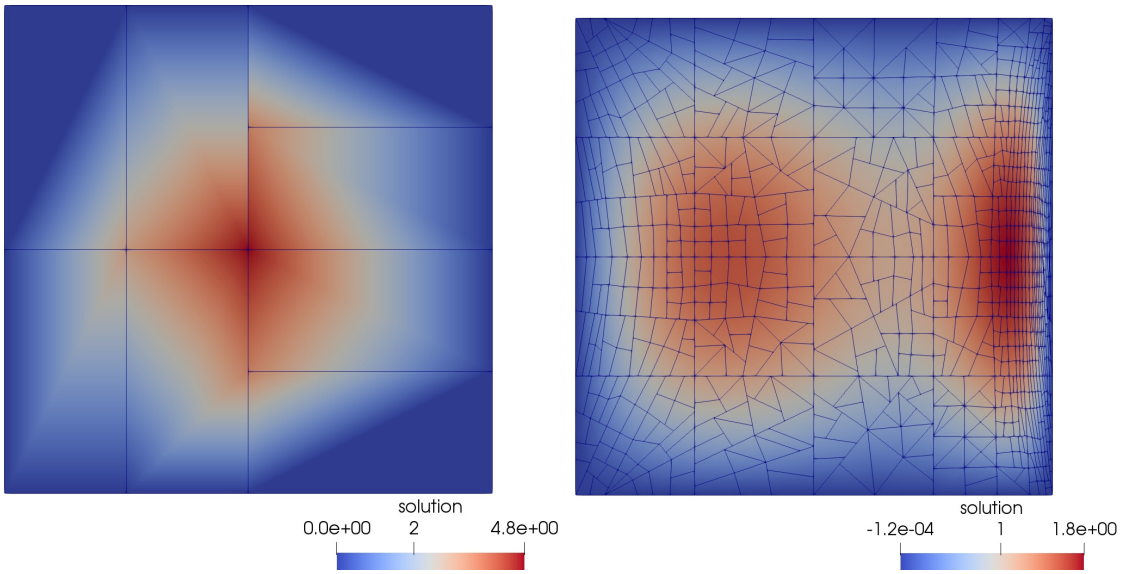

(a) VEM of order 1. Adaptive step n. 1.

(b) VEM of order 1. Adaptive step n. 17.

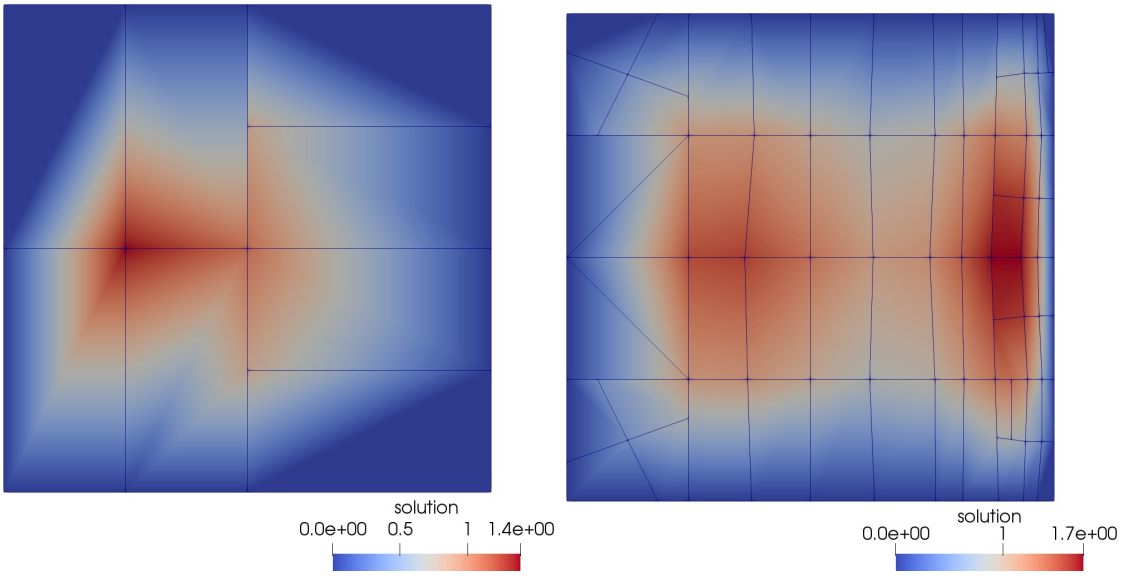

(c) VEM order 2. Adaptive step n. 1.

(d) VEM order 2. Adaptive step n. 9.

FIG. 16: Test case 3. Computed solutions and corresponding anisotropic grids at different steps of the adaptive algorithm based on employing the *heuristically scaled estimator* η_h^{heur} defined in (6.5) to drive the adaptive algorithm.

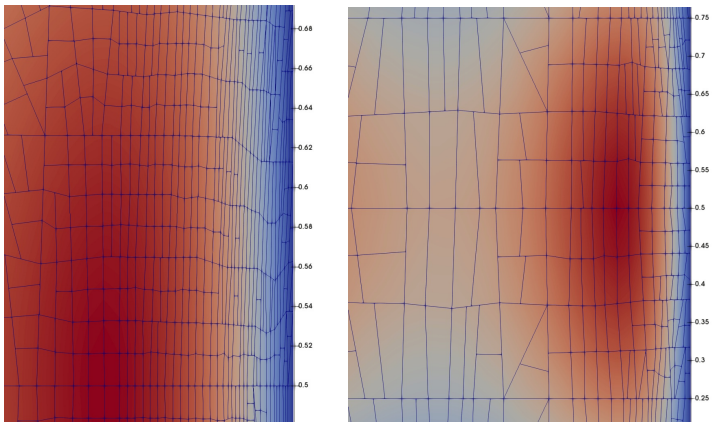

(a) VEM order 1. Adaptive step n. 21.

(b) VEM order 2. Adaptive step n. 18

FIG. 17: Test case 3. Zoom of the computed solutions and corresponding anisotropic grids at the final step of the adaptive algorithm based on employing the *heuristically scaled estimator* η_h^{heur} defined in (6.5) to drive the adaptive algorithm.

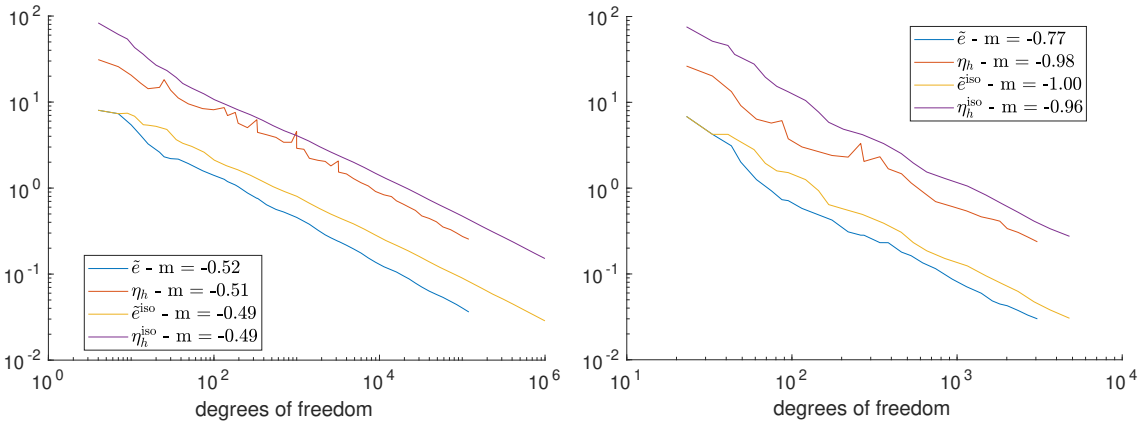

(a) VEM of order 1.

(b) VEM of order 2.

FIG. 18: Test case 3. Computed values of the estimator η_h, computed errors $\widetilde{e}$ based on employing the exact solution, and corresponding computed convergence rates $\mathtt{m}$ as a function of the number of degrees of freedom. The results are compared with the analogous quantities obtained based on employing the isotropic error estimator η_h^{iso} defined in (6.4).

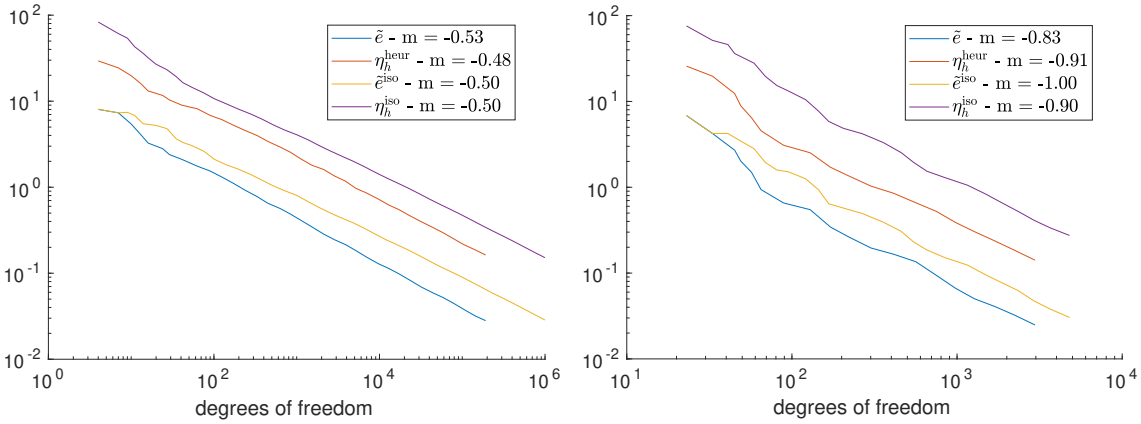

(a) VEM of order 1. (b) VEM of order 2.

FIG. 19: Test case 3. Computed values of the estimator η_h^{heur}, computed errors $\widetilde{e}$ based on employing the exact solution, and corresponding computed convergence rates $\mathtt{m}$ as a function of the number of degrees of freedom. The results are compared with the analogous quantities obtained based on employing the isotropic error estimator η_h^{iso} defined in (6.4).

A. Appendix

PROPOSITION A.1 Under Assumption 3.6, there holds

$$|\hat{z}|_{H^1(\hat{\omega})} \lesssim \|\hat{z}\|_{L^2(\hat{\omega})} \quad \forall \hat{z} \in \hat{\Theta}(\hat{\omega})/\mathbb{R} \tag{A.1}$$

$$\|\hat{z}\|_{L^\infty(\hat{\omega})} \lesssim \|\hat{z}\|_{L^2(\hat{\omega})} \quad \forall \hat{z} \in \hat{\Theta}(\hat{\omega}) \tag{A.2}$$

where the constants do not depend on the specific choice of the patch $\hat{\omega}$.

Proof. Employing the standard arguments in the proof of the well known result that on finite dimensional spaces all norms are equivalent we obtain

$$|\hat{z}|_{H^1(\hat{\omega})} \leqslant \frac{\sqrt{N}\max_i |\hat{\varphi}_i|_{H^1(\hat{\omega})}}{\min_{\hat{\Theta}(\hat{\omega})\ni\hat{w}=\sum_{i=1}^N \hat{w}_i\hat{\varphi}_i:\ \sum_{i=1}^N \hat{w}_i^2=1} \|\hat{w}\|_{L^2(\hat{\omega})}} \|\hat{z}\|_{L^2(\hat{\omega})} \tag{A.3}$$

$$\|\hat{z}\|_{L^\infty(\hat{\omega})} \leqslant \frac{\sqrt{N}\max_i \|\hat{\varphi}_i\|_{L^\infty(\hat{\omega})}}{\min_{\hat{\Theta}(\hat{\omega})\ni\hat{w}=\sum_{i=1}^N \hat{w}_i\hat{\varphi}_i:\ \sum_{i=1}^N \hat{w}_i^2=1} \|\hat{w}\|_{L^2(\hat{\omega})}} \|\hat{z}\|_{L^2(\hat{\omega})} \tag{A.4}$$

where $\hat{\Theta}(\hat{\omega}) = \text{span}\{\hat{\varphi}_1, \dots \hat{\varphi}_N\}$ and φ_i is the associated ith virtual basis function.

As in the Virtual Element Method, differently from the Finite Element Method, there is no unique reference element $\hat{K}$ that can be employed independently of the physical element K, we need to prove that the constants appearing in (A.3)-(A.4) are uniform with respect to $\hat{\omega}$. To this aim, we follow the proofs of (Cangiani *et al.*, 2017a, Lemma 4.9) and (Beirão da Veiga & Manzini, 2015b, Theorem 4.1). First, we note that in view of Proposition 3.5 the number N is uniformly bounded with respect to $\hat{\omega}$. We denote by N^* this uniform constant. To proceed, we let $\hat{X} = \{\hat{X}_1, \dots, \hat{X}_N\}$ for all $N \leqslant N^*$ denote the coordinates of the vertices of the elements in the patch $\hat{\omega}$ and we employ the symbol $\hat{\Sigma}$ to refer to the set of all possible configurations of the N vertices.

Having in mind (A.3), we set

$$C(\hat{X}) := \frac{\max_i |\hat{\varphi}_i|_{H^1(\hat{\omega})}}{\min_{\hat{\Theta}(\hat{\omega})\ni\hat{w}=\sum_{i=1}^N \hat{w}_i\hat{\varphi}_i:\ \sum_{i=1}^N \hat{w}_i^2=1} \|\hat{w}\|_{L^2(\hat{\omega})}}.$$

If the following are true:

(a) $C(\hat{X})$ is a continuous function on $\hat{\Sigma}$;

(b) $\hat{\Sigma}$ is a compact set;

then $C = \text{argmax}_{\hat{X}\in\hat{\Sigma}} C(\hat{X})$ exists and $C\sqrt{N^*}$ is the uniform constant in (A.1). The validity of (a) is obtained following the arguments in the proofs of (Cangiani *et al.*, 2017a, Lemma 4.9) and (Beirão da Veiga & Manzini, 2015b, Theorem 4.1). In particular, the continuity of $C(\hat{X})$ essentially relies on the continuity of the solution of harmonic problems with respect to the boundary data and with respect to the deformation of the domain. The validity of (b) is a consequence of our regularity assumptions for the reference elements (cf. (Cangiani *et al.*, 2017a, Lemma 4.9) and (Beirão da Veiga & Manzini, 2015b, Theorem 4.1)).

An analogous argument can be employed to prove (A.4). In this respect, note that $\|\hat{\varphi}_i\|_{L^\infty(\hat{\omega})} = 1$ for every $i = 1,\dots,N$. □

Acknowledgments

We want to thank the anonymous Referee for her/his insightful comments that led to a substantial improvement of the paper.

P.F.A., S.B., A.B., A.D., and M.V. acknowledge the financial support of MIUR through the PRIN grant n. 201744KLJL. P.F.A., S.B., A.B., A.D., and M.V. have also been funded by INdAM-GNCS. S.B., A.B., and A.D. also acknowledge the financial support of MIUR through the project "Dipartimenti di Eccellenza 2018-2022" (CUP E11G18000350001).

REFERENCES

ADAMS, R. A. & FOURNIER, J. J. F. (2003) *Sobolev spaces*. Pure and Applied Mathematics (Amsterdam), vol. 140, second edn. Elsevier/Academic Press, Amsterdam, pp. xiv+305.

ANTONIETTI, P. F., BEIRÃO DA VEIGA, L., LOVADINA, C. & VERANI, M. (2013) Hierarchical a posteriori error estimators for the mimetic discretization of elliptic problems. *SIAM J. Numer. Anal.*, **51**, 654–675.

ANTONIETTI, P. F., BERRONE, S., VERANI, M. & WEISSER, S. (2019) The virtual element method on anisotropic polygonal discretizations. *Lecture Notes in Computational Science and Engineering*, **126**, 725–733.

APEL, T. (1999) *Anisotropic finite elements: local estimates and applications*. Advances in Numerical Mathematics. B. G. Teubner, Stuttgart.

BEIRÃO DA VEIGA, L. (2008) A residual based error estimator for the mimetic finite difference method. *Numer. Math.*, **108**, 387–406.

BEIRÃO DA VEIGA, L., BREZZI, F., MARINI, L. D. & RUSSO, A. (2016) Virtual element method for general second-order elliptic problems on polygonal meshes. *Mathematical Models and Methods in Applied Sciences*, **26**, 729–750.

BEIRÃO DA VEIGA, L., LOVADINA, C. & RUSSO, A. (2017) Stability analysis for the virtual element method. *Math. Models Methods Appl. Sci.*, **27**, 2557–2594.

BEIRÃO DA VEIGA, L., MANZINI, G. & MASCOTTO, L. (2019) A posteriori error estimation and adaptivity in *hp* virtual elements. *Numer. Math.*, **143**, 139–175.

BEIRÃO DA VEIGA, L. & ERN, A. (2016) Preface [Special issue—Polyhedral discretization for PDE]. *ESAIM Math. Model. Numer. Anal.*, **50**, 633–634.

BEIRÃO DA VEIGA, L. & MANZINI, G. (2008) An a posteriori error estimator for the mimetic finite difference approximation of elliptic problems. *Internat. J. Numer. Methods Engrg.*, **76**, 1696–1723.

BEIRÃO DA VEIGA, L. & MANZINI, G. (2015a) Residual *a posteriori* error estimation for the virtual element method for elliptic problems. *ESAIM Math. Model. Numer. Anal.*, **49**, 577–599.

BEIRÃO DA VEIGA, L. & MANZINI, G. (2015b) Residual *a posteriori* error estimation for the virtual element method for elliptic problems. *ESAIM Math. Model. Numer. Anal.*, **49**, 577–599.

BEIRÃO DA VEIGA, L., BREZZI, F., CANGIANI, A., MANZINI, G., MARINI, L. & RUSSO, A. (2013) Basic principles of Virtual Element Methods. *Mathematical Models and Methods in Applied Sciences*, **23**, 199–214.

BERNARDI, C. & GIRAULT, V. (1998) A local regularization operator for triangular and quadrilateral finite elements. *SIAM J. Numer. Anal.*, **35**, 1893–1916.

BERRONE, S., BORIO, A. & D'AURIA, A. (2019) Refinement strategies for polygonal meshes applied to adaptive vem discretization. arXiv:1912.05403.

BERRONE, S. & BORIO, A. (2017) A residual *a posteriori* error estimate for the Virtual Element Method. *Math. Models Methods Appl. Sci.*, **27**, 1423–1458.

CANGIANI, A., MANZINI, G. & SUTTON, O. J. (2017a) Conforming and nonconforming virtual element methods for elliptic problems. *IMA J. Numer. Anal.*, **37**, 1317–1354.

CANGIANI, A., GEORGOULIS, E. H., PRYER, T. & SUTTON, O. J. (2017b) A posteriori error estimates for the virtual element method. *Numer. Math.*, **137**, 857–893.

CANGIANI, A. & MUNAR, M. (2019) A posteriori error estimates for mixed virtual element methods. arXiv:1904.10054.

CAO, S. & CHEN, L. (2019) Anisotropic error estimates of the linear nonconforming virtual element methods. *SIAM J. Numer. Anal.*, **57**, 1058–1081.

CHEN, L. & HUANG, J. (2018) Some error analysis on virtual element methods. *Calcolo*, **55**, Art. 5, 23.

CHI, H., BEIRÃO DA VEIGA, L. & PAULINO, G. H. (2019) A simple and effective gradient recovery scheme and *a posteriori* error estimator for the virtual element method (VEM). *Comput. Methods Appl. Mech. Engrg.*, **347**, 21–58.

DI PIETRO, D. A. & SPECOGNA, R. (2016) An a posteriori-driven adaptive mixed high-order method with application to electrostatics. *J. Comput. Phys.*, **326**, 35–55.

FORMAGGIA, L. & PEROTTO, S. (2001) New anisotropic a priori error estimates. *Numer. Math.*, **89**, 641–667.

FORMAGGIA, L. & PEROTTO, S. (2003) Anisotropic error estimates for elliptic problems. *Numer. Math.*, **94**, 67–92.

GEORGOULIS, E. H. (2003) Discontinuous galerkin methods on shape-regular and anisotropic meshes. *Ph.D. thesis*, Computing Laboratory, University of Oxford.

GEORGOULIS, E. H. (2006) *hp*–version interior penalty discontinuous Galerkin finite element methods on anisotropic meshes. *International Journal of Numerical Analysis and Modeling*, **3**, 52–79.

GEORGOULIS, E. H., HALL, E. & HOUSTON, P. (2007a) Discontinuous Galerkin methods for advection-diffusion-reaction problems on anisotropically refined meshes. **30**, 246–271.

GEORGOULIS, E. H., HALL, E. & HOUSTON, P. (2007b) Discontinuous Galerkin methods on *hp*-anisotropic meshes i: a priori error analysis. **1**, 221–244.

GEORGOULIS, E. H., HALL, E. & HOUSTON, P. (2009) Discontinuous Galerkin methods on *hp*-anisotropic meshes. II. A posteriori error analysis and adaptivity. *Appl. Numer. Math.*, **59**, 2179–2194.

GUO, H., XIE, C. & ZHAO, R. (2019) Superconvergent gradient recovery for virtual element methods. *Mathematical Models and Methods in Applied Sciences*, **29**, 2007–2031.

HABASHI, W. G., DOMPIERRE, J., BOURGAULT, Y., AIT-ALI-YAHIA, D., FORTIN, M. & VALLET, M.-G. (2000) Anisotropic mesh adaptation: towards user-independent, mesh-independent and solver-independent cfd. part i: general principles. *International Journal for Numerical Methods in Fluids*, **32**, 725–744.

MORA, D., RIVERA, G. & RODRÍGUEZ, R. (2017) A posteriori error estimates for a virtual element method for the Steklov eigenvalue problem. *Comput. Math. Appl.*, **74**, 2172–2190.

MU, L. (2019) Weak Galerkin based a posteriori error estimates for second order elliptic interface problems on polygonal meshes. *J. Comput. Appl. Math.*, **361**, 413–425.

NOCHETTO, R. H. & VEESER, A. (2012) Primer of adaptive finite element methods. *Multiscale and adaptivity: modeling, numerics and applications*. Lecture Notes in Math., vol. 2040. Springer, Heidelberg, pp. 125–225.

VACCA, G. (2018) An H^1-conforming virtual element for Darcy and Brinkman equations. *Math. Models Methods Appl. Sci.*, **28**, 159–194.

VERFÜRTH, R. (2013) *A posteriori error estimation techniques for finite element methods*. Numerical Mathematics and Scientific Computation. Oxford University Press, Oxford, pp. xx+393.

VOHRALÍK, M. & YOUSEF, S. (2018) A simple a posteriori estimate on general polytopal meshes with applications to complex porous media flows. *Comput. Methods Appl. Mech. Engrg.*, **331**, 728–760.

WEISSER, S. (2011) Residual error estimate for BEM-based FEM on polygonal meshes. *Numer. Math.*, **118**, 765–788.

WEISSER, S. (2017) Residual based error estimate and quasi-interpolation on polygonal meshes for high order BEM-based FEM. *Comput. Math. Appl.*, **73**, 187–202.

WEISSER, S. (2019) Anisotropic polygonal and polyedral discretizations in finite element analysis. *ESAIM: Mathematical Modelling and Numerical Analysis*, **53**, 475–501.

WEISSER, S. (2019) *BEM-based Finite Element Approaches on Polytopal Meshes*. Lecture Notes in Computational Science and Engineering, vol. 130. Springer International Publishing.

WEISSER, S. & WICK, T. (2018) The dual-weighted residual estimator realized on polygonal meshes. *Comput. Methods Appl. Math.*, **18**, 753–776.

ZENONI, G., LEICHT, T., COLOMBO, A. & BOTTI, L. (2017) An agglomeration-based adaptive discontinuous Galerkin method for compressible flows. *Internat. J. Numer. Methods Fluids*, **85**, 465–483.

ZHU, J. Z. & ZIENKIEWICZ, O. C. (1990) Superconvergence recovery technique and a posteriori error estimators. *International Journal for Numerical Methods in Engineering*, **30**, 1321–1339.

ZIENKIEWICZ, O. C. & ZHU, J. Z. (1992a) The superconvergent patch recovery and a posteriori error estimates. part 1: The recovery technique. *International Journal for Numerical Methods in Engineering*, **33**, 1331–1364.

ZIENKIEWICZ, O. C. & ZHU, J. Z. (1992b) The superconvergent patch recovery and a posteriori error estimates. part 2: Error estimates and adaptivity. *International Journal for Numerical Methods in Engineering*, **33**, 1365–1382.